JOURNAL OF GEOPHYSICAL RESEARCH, VOL. 114, D20115, doi:10.1029/2009JD012239, 2009

Evolution of the quasi 2-day wave during January 2006

J. P. McCormack,[1] L. Coy,[1] and K. W. Hoppel[2]

Received 13 April 2009; revised 6 July 2009; accepted 27 July 2009; published 28 October 2009.

[1] We examine the evolution of the quasi 2-day wave in the middle atmosphere during the period from 5 January to 5 February 2006 using global synoptic meteorological fields from the high-altitude Navy Operational Global Atmospheric Prediction System Advanced Level Physics, High Altitude (NOGAPS-ALPHA) forecast-assimilation system. This period is characterized by a high level of planetary wave activity in the Northern Hemisphere (winter) extratropical stratosphere prior to a sudden stratospheric warming (SSW) on 20 January 2006. Space-time spectral analysis of 6-hourly NOGAPS-ALPHA fields finds the largest quasi 2-day wave amplitudes in the Southern Hemisphere (summer) extratropical upper mesosphere. Eliassen-Palm flux diagnostics indicate that this extratropical quasi 2-day wave is related to baroclinic instability along the equatorward flank of the summer easterly jet. The quasi 2-day wave is also evident in NOGAPS-ALPHA water vapor fields near the tropical stratopause and is related to barotropic instability. We find that the strong planetary wave activity leading up to the SSW produced an enhanced northward component of the residual meridional circulation that influenced the background zonal winds and, by extension, the quasi 2-day wave forcing in both the tropical and extratropical regions. In the tropical region, the combination of enhanced horizontal momentum advection by the residual meridional circulation and inertially unstable circulations related to planetary wave breaking in the subtropics produced conditions favoring barotropic instability. In the extratropical region, the enhanced residual meridional circulation altered the zonal wind tendency through increased Coriolis torque.

Citation: McCormack, J. P., L. Coy, and K. W. Hoppel (2009), Evolution of the quasi 2-day wave during January 2006, *J. Geophys. Res.*, *114*, D20115, doi:10.1029/2009JD012239.

1. Introduction

[2] Observations of middle atmospheric winds, temperatures, and constituents have long documented a prominent westward-propagating zonal wave number 3 feature with a period of approximately 2 days occurring in the summer hemisphere near solstice [e.g., *Muller and Nelson*, 1978; *Coy*, 1979; *Rodgers and Prata*, 1981; *Salby*, 1981; *Randel*, 1993]. This feature is often referred to as the 2-day wave or, more accurately, the quasi 2-day wave (Q2DW). This paper presents the first detailed study of the Q2DW with a global data assimilation system, the high-altitude Navy Operational Global Atmospheric Prediction System (NOGAPS-ALPHA) [*Hoppel et al.*, 2008; *Eckermann et al.*, 2009]. Space-time spectral analysis of NOGAPS-ALPHA temperature, horizontal wind, and water vapor fields during January 2006 confirms existing theories of Q2DW formation and offers new insight into the physical processes linking the Q2DW in the summer mesosphere with planetary wave activity in the winter stratosphere.

[3] The Q2DW in both meridional wind and temperature is most pronounced at summer midlatitudes but can extend across the equator into the winter subtropics during periods shortly after summer solstice [*Harris*, 1994; *Wu et al.*, 1993]. The Q2DW has also been observed in middle atmospheric water vapor (H_2O) [*Limpasuvan and Leovy*, 1995; *Limpasuvan and Wu*, 2003]. The long photochemical lifetime of H_2O in the upper stratosphere and mesosphere compared to transport time scales makes it particularly well-suited for identifying the zonal structure of the Q2DW [see, e.g., *Limpasuvan and Wu*, 2003] throughout the middle atmosphere. To illustrate this point, Figure 1 plots synoptic maps of analyzed NOGAPS-ALPHA H_2O at 0.01 hPa on 15 January 2006 (Figure 1a), and at 1 hPa on 26 January 2006 (Figure 1b). Animated loops of the NOGAPS-ALPHA H_2O fields at these two levels throughout the month of January 2006 are available in Animations S1 and S2 in the auxiliary material.[1]

[4] The theory explaining the origin and structure of the Q2DW has been well established. *Salby* [1981] demonstrated that the space-time characteristics of the Q2DW are closely related to a global normal (resonant) mode. Subsequently, *Plumb* [1983] proposed that baroclinic instability near the core of a typical summertime easterly jet can trigger the growth of this type of disturbance. Both satellite-based

[1] Space Science Division, Naval Research Laboratory, Washington, D. C., USA.
[2] Remote Sensing Division, Naval Research Laboratory, Washington, D. C., USA.

[1] Auxiliary materials are available with the full article. doi:10.1029/2009JD012239.

Report Documentation Page

Form Approved
OMB No. 0704-0188

1. REPORT DATE	2. REPORT TYPE	3. DATES COVERED
06 JUL 2009		**00-00-2009 to 00-00-2009**

4. TITLE AND SUBTITLE	5a. CONTRACT NUMBER
Evolution of the quasi 2-day wave during January 2006	5b. GRANT NUMBER
	5c. PROGRAM ELEMENT NUMBER
6. AUTHOR(S)	5d. PROJECT NUMBER
	5e. TASK NUMBER
	5f. WORK UNIT NUMBER
7. PERFORMING ORGANIZATION NAME(S) AND ADDRESS(ES) **Naval Research Laboratory,Space Science Division,Washington,DC,20375**	8. PERFORMING ORGANIZATION REPORT NUMBER
9. SPONSORING/MONITORING AGENCY NAME(S) AND ADDRESS(ES)	10. SPONSOR/MONITOR'S ACRONYM(S)
	11. SPONSOR/MONITOR'S REPORT NUMBER(S)

12. DISTRIBUTION/AVAILABILITY STATEMENT
Approved for public release; distribution unlimited

13. SUPPLEMENTARY NOTES

14. ABSTRACT

15. SUBJECT TERMS

16. SECURITY CLASSIFICATION OF:			17. LIMITATION OF ABSTRACT	18. NUMBER OF PAGES	19a. NAME OF RESPONSIBLE PERSON
a. REPORT **unclassified**	b. ABSTRACT **unclassified**	c. THIS PAGE **unclassified**	**Same as Report (SAR)**	**19**	

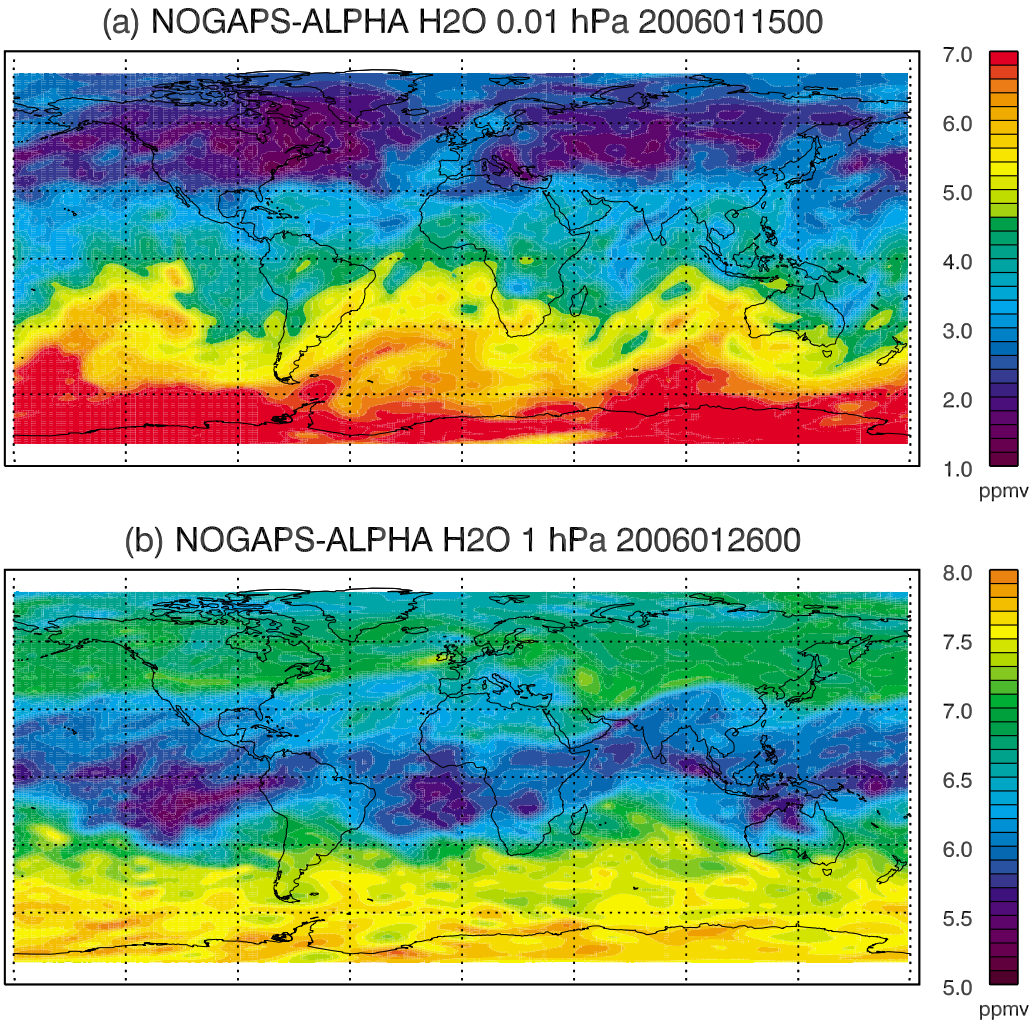

Figure 1. NOGAPS-ALPHA water vapor mixing ratios at (a) 0.01 hPa for 0000 UTC 15 January 2006 and (b) 1 hPa for 0000 UTC 26 January 2006 at 1 hPa.

observations [e.g., *Randel*, 1993; *Limpasuvan and Leovy*, 1995; *Lieberman*, 1999; *Limpasuvan and Wu*, 2003; *Garcia et al.*, 2005] and middle atmospheric modeling studies [e.g., *Norton and Thuburn*, 1999; *Limpasuvan et al.*, 2000a; *Salby and Callaghan*, 2001; *Richter et al.*, 2008] have confirmed that the Q2DW is triggered by amplifying transient waves from localized baroclinic or barotropic instabilities whose space-time characteristics project onto the global normal mode. These instabilities are located in regions where the meridional gradient of potential vorticity is negative.

[5] The largest Q2DW amplitudes tend to occur within regions of high vertical wind shear above the core of the extratropical mesospheric summer easterly jet. The high vertical wind shears are maintained by the effects of breaking gravity waves [see, e.g., *Garcia et al.*, 2005]. The Q2DW is also observed in barotropically unstable regions associated with strong meridional curvature in zonal wind near the summer subtropical stratopause. These regions often form as a result of inertially unstable circulations related to the intrusion of quasi-stationary planetary waves into the subtropics [*Sassi et al.*, 1993; *Orsolini et al.*, 1997].

[6] The goal of the present study is to examine possible mechanisms explaining the observed episodic behavior of the Q2DW during the January 2006 period. Past observational and modeling studies [e.g., *Orsolini et al.*, 1997; *Limpasuvan et al.*, 2000a, 2000b] have linked the evolution of the Q2DW near the subtropical stratopause during austral summer with planetary wave breaking in the winter stratosphere. It has also been suggested that planetary wave activity in the winter hemisphere may influence the behavior of the Q2DW through an intensification of the mean meridional circulation [*Limpasuvan et al.*, 2000b; *Salby and Callaghan*, 2003]. The NOGAPS-ALPHA data assimilation system provides the first opportunity to examine these theories using global synoptic meteorological analyses of the upper stratosphere and mesosphere obtained from assimilation of temperature and constituents from more than one satellite data set. In this regard, it offers distinct advantages over earlier observational studies of the Q2DW that used asynoptic satellite measurements of the middle atmosphere from a single instrument [*Wu et al.*, 1993; *Lieberman*, 1999; *Limpasuvan and Wu*, 2003; *Garcia et al.*, 2005].

[7] The present study focuses on the January 2006 period, which is of particular interest due to the occurrence of a major stratospheric sudden warming (SSW) in the Northern Hemisphere on 20 January. Prior to the SSW, there was a marked increase in planetary wave activity in the winter midlatitude stratosphere. We present evidence that this enhanced

planetary wave activity prior to the SSW had a global impact on the Q2DW in middle atmospheric winds, temperatures, and water vapor.

[8] Section 2 provides a description of the NOGAPS-ALPHA forecast model and data assimilation components. Section 3 describes the data analysis methods. Section 4 presents a detailed description of the Q2DW and its sources during January 2006. Section 5 discusses the connection between planetary wave activity in the winter stratosphere and the evolution of the Q2DW during January 2006. Section 6 summarizes our results and outlines future research.

2. NOGAPS-ALPHA Description

[9] The Navy Operational Global Atmospheric Prediction System (NOGAPS) combines a global spectral forecast model [*Hogan and Rosmond*, 1991] with the three-dimensional NRL Variational Data Assimilation (NAVDAS) [*Daley and Barker*, 2001] to produce global meteorological fields every 6 hours. An advanced-level physics high-altitude (ALPHA) prototype of NOGAPS now extends from the surface to ~100 km altitude. The vertical domain of NOGAPS-ALPHA has recently been extended to the upper mesosphere/lower thermosphere region (~100 km) [*Hoppel et al.*, 2008]. This study uses NOGAPS-ALPHA meteorological analyses of the middle atmosphere for the January 2006 period based on temperature and constituent measurements from the Aura Microwave Limb Sounder (MLS) and TIMED Sounding of the Atmosphere by Broadband Emission of Radiation (SABER) instruments.

[10] The new NOGAPS-ALPHA analyses offer several distinct advantages for studying the quasi 2-day wave: (1) NOGAPS-ALPHA generates global synoptic fields of meteorological variables that include both directly assimilated quantities (e.g., temperature and constituents) and derived quantities (e.g., zonal and meridional winds, divergence, vertical velocity). (2) The forecast model component with a comprehensive middle atmospheric physics package essentially "fills" gaps in the assimilated data. (3) Information from more than one observational platform can be included.

[11] Sections 2.1 and 2.2 present brief overviews of NOGAPS-ALPHA forecast model and data assimilation components. For a more complete description of NOGAPS-ALPHA, see *McCormack et al.* [2006], *Hoppel et al.* [2008], and *Eckermann et al.* [2009].

2.1. Forecast Model Component

[12] The forecast model component of NOGAPS-ALPHA has an Eulerian hydrostatic dynamical core that is spectral in the horizontal domain and employs energy- and angular momentum–conserving finite differencing in the vertical domain based on a generalized vertical coordinate [*Hogan and Rosmond*, 1991]. The global spectral forecast model can operate with a variety of horizontal and vertical resolutions depending on specific operational or research requirements. For the present study, the forecast model adopts a triangular truncation up to the first 79 wave numbers (T79), with a horizontal grid spacing of 1.5° in longitude and latitude on a quadratic Gaussian grid. The model vertical grid consists of 68 (L68) hybrid $\sigma - p$ levels [*Eckermann*, 2009] with a top at 5×10^{-4} hPa and ~2 km spacing of levels throughout most of the stratosphere and lower mesosphere.

[13] Shortwave heating and longwave cooling rates due to O_3, CO_2, and H_2O from the surface to the lower mesosphere are computed using the method of *Chou et al.* [2001] and *Chou and Suarez* [2002]. Additional CO_2 cooling rate calculations are performed using the parameterization of *Fomichev et al.* [1998] for the upper mesospheric region where the effects of nonlocal thermodynamic equilibrium begin to dominate.

[14] Both O_3 and H_2O are prognostic variables in the NOGAPS-ALPHA system. The model employs linearized parameterization of the gas-phase photochemistry for both O_3 [*McCormack et al.*, 2006] and H_2O [*McCormack et al.*, 2008]. The parameterized photochemistry provides an important constraint on the model O_3 and H_2O fields that maintains observed horizontal and vertical gradients throughout the middle atmosphere. This is of particular importance for modeling the Q2DW in mesospheric H_2O, which arises from the effects of meridional wind perturbations superimposed on the spatial gradients in the background (i.e., zonal mean) H_2O field.

[15] The model's T79 spectral truncation does not provide sufficient horizontal resolution to resolve gravity wave breaking explicitly in the middle atmosphere. This effect consists mainly of a drag force on the background winds that is a major source of momentum driving the circulation of the upper stratosphere and mesosphere away from a thermal equilibrium state. The model uses the parameterizations of *Palmer et al.* [1986] and *Garcia et al.* [2007] to describe the effects of sub-grid-scale orographic and nonorographic gravity wave drag, respectively.

2.2. Data Assimilation Component

[16] The data assimilation component of NOGAPS-ALPHA is based on the NRL Atmospheric Variational Data Assimilation System (NAVDAS) [*Daley and Barker*, 2001]. NAVDAS is a 3DVAR system with a 6-h update cycle that assimilates both conventional ground-based observations (e.g., wind, pressure, temperature from station reports and radiosondes) and satellite-based observations (e.g., microwave radiances, surface winds, precipitable water). In the present study, NOGAPS-ALPHA assimilates Aura MLS Version 2.2 temperature, O_3, and H_2O profile measurements [*Lambert et al.*, 2007; *Schwartz et al.*, 2008], as described in the work of *Hoppel et al.* [2008]. The Aura satellite completes ~13 orbits per day with coverage between 82°S and 82°N latitude. NOGAPS-ALPHA also assimilates Version 1.07 temperature profile measurements from the TIMED SABER instrument [*Remsberg et al.*, 2008]. SABER is a side-viewing instrument whose coverage alternates every 2 months between the pole in one hemisphere and ~52° latitude in the opposite hemisphere. TIMED switched from south-viewing to north-viewing mode on 13 January 2006. This change in coverage is not seen to affect the Q2DW in the NOGAPS-ALPHA analyses.

[17] Temperature profiles from both MLS and SABER instruments are assimilated between the 32 and 0.002 hPa pressure levels. The precision of individual MLS temperature retrievals ranges from <1 K in the stratosphere to ~3 K in the upper mesosphere [*Schwartz et al.*, 2008], which is comparable to the SABER temperature retrievals [e.g.,

Hoppel et al., 2008]. The vertical resolution of the SABER temperature retrieval (determined from the full width at half maximum of the instrument averaging kernels) remains ~2 km throughout the stratosphere and mesosphere while the resolution of the MLS temperature retrieval degrades from ~3 km in the stratosphere to ~13 km near the 0.01 hPa level. Global mean systematic biases on the order of 2–3 K exist between the MLS and SABER temperatures, which have been removed prior to assimilation to avoid introducing spurious spatial variability into the temperature analyses, as described in the work of *Hoppel et al.* [2008].

[18] NOGAPS-ALPHA mesospheric water vapor analyses are based on assimilation of Aura MLS Version 2.2 profile measurements. The Version 2.2 MLS H_2O retrievals have an improved precision in the mesosphere compared to earlier versions, ranging from 0.4 to 1.1 ppmv between the 0.1 and 0.01 pressure levels, while the vertical resolution degrades from ~3 km in the stratosphere to values between 12 and 16 km in the mesosphere [*Lambert et al.*, 2007]. In the present study, daily MLS H_2O profiles are assimilated between 300 and 0.002 hPa as described in the study of *Eckermann et al.* [2009].

[19] In addition to temperature and water vapor, horizontal winds and their divergence are also standard NOGAPS-ALPHA output fields. Although the assimilation does not include any middle atmospheric wind measurements, NAVDAS calculates correlated temperature and wind increments based on a gradient wind approximation in the off-diagonal elements of the observation error covariance matrix. The assimilated wind and temperature fields are further constrained by the physical parameterizations of the atmospheric model (e.g., gravity wave drag, diffusion). Vertical winds are inferred from NOGAPS-ALPHA horizontal divergence fields through vertical integration of the continuity equation.

3. Data Analysis

[20] Space-time spectral analysis [*Hayashi*, 1971] is used to isolate the Q2DW from other planetary-scale wave modes in the middle atmosphere. In this study, we employ a two-dimensional fast Fourier transform (2DFFT) to describe the features of the Q2DW in the NOGAPS-ALPHA analyses during January 2006. In the 2DFFT approach, an observed time series $W(x, t)$ (representing temperature, water vapor mixing ratio, meridional wind, etc.) that is periodic in longitude x for the time period $0 < t < T$ can be expanded as a Fourier series in space and time

$$W(x,t) = Re\sum_{k,w}\left[\hat{W}_{k,w}e^{i(kx+\omega t)} + \hat{W}_{k,-\omega}e^{i(kx-\omega t)}\right], \qquad (1)$$

where $\hat{W}_{k,\omega}$ is the Fourier transform

$$\hat{W}_{k,\omega} = \frac{1}{2\pi T}\int_0^T\left[\int_0^{2\pi} W(x,t)e^{-ikx}dx\right]e^{-i\omega t}dt, \qquad (2)$$

with ω and k representing angular frequency and horizontal wave number, respectively.

[21] NOGAPS-ALPHA fields generated every 6 hours for the period 5 January to 5 February 2006 are analyzed with the 2DFFT, giving 128 data points in time and 360 points in longitude. The sampling rate of four times each day gives a Nyquist frequency of 2 cpd. Prior to performing the 2DFFT, the daily zonal means are subtracted from each field at each pressure level and latitude. A cosine taper is applied to the first and last 10% of each record in time. Upon computing the Fourier transform, a three-point smoothing is applied to the coefficients in the frequency domain.

[22] The space-time power spectrum $P(k, \omega) = |\hat{W}_{k,\omega}|^2$ can be used to describe the amount of variance at each frequency and wave number through Parseval's Theorem. Cross-spectral analysis [e.g., *von Storch and Zwiers*, 1999] is applied to determine how closely related two space-time spectra are related within a spectral band of interest. Where the spectra exhibit a high level of coherence, we can be confident that we are observing a real phenomenon and not an artifact due to poor spatial or temporal sampling. Specifically, we compute the squared coherency coh^2 [*Hayashi*, 1971] between the spectra at different latitudes and pressure levels for westward zonal wave 3 between 0.4 and 0.6 cpd. Using the method of *Madden and Julian* [1971], we estimate the statistical significance of coh^2 assuming 5 degrees of freedom in the 2DFFT spectra. This is based on the length of the data record (128 points), the Nyquist frequency of 2 cpd, and an a priori estimate of 0.1 cpd spectral resolution to resolve the Q2DW. Significance levels of coh^2 are then determined from Table 1 of *Thompson* [1979].

[23] Figure 2 plots the normalized space-time power spectra of the NOGAPS-ALPHA temperature and H_2O fields at 40°S and 0.01 hPa during the period from 5 January to 5 February 2006. Only the portion of the time spectrum representing westward propagation is plotted since there is negligible power at eastward frequencies. The spectra indicate that the variance in these fields peaks sharply at wave number 3 and frequencies between 0.4 and 0.6 cpd (periods of 2.5 and 1.7 days, respectively). Based on this result, we can isolate the Q2DW in the NOGAPS-ALPHA meteorological fields using an inverse Fourier transform after applying a band-pass filter for zonal wave number 3 and frequencies between 0.4 and 0.6 cpd.

[24] To illustrate this capability, Figure 3 shows the vertical Q2DW structure in NOGAPS-ALPHA temperature, water vapor, meridional wind, and vertical wind fields at 40°S on 17 January 2006 obtained from the filtered spectra. We note that the phase of the temperature Q2DW (Figure 3a) exhibits a pronounced westward tilt with height above the 0.1 hPa level at this location, in agreement with earlier studies. This feature is also seen to some degree in the meridional wind Q2DW, but not in the corresponding results for H_2O and w. We find that the vertical structure of the Q2DW is not fixed, but instead varies with latitude and time throughout the month. For example, Figure 4 shows the Q2DW structure on 25 January at 20°S. Significant differences are seen in the temperature, water vapor, and vertical velocity fields. Specifically, the westward phase tilt in the subtropical temperature field is present only above the 0.01 hPa level. In addition, both the H_2O and w fields at 20°S show two distinct regions of Q2DW activity near 1 hPa and 0.01 hPa that are out of phase.

[25] Overall, the spectral characteristics of the Q2DW in NOGAPS-ALPHA temperature during January 2006 are quite similar to the results reported in the study by

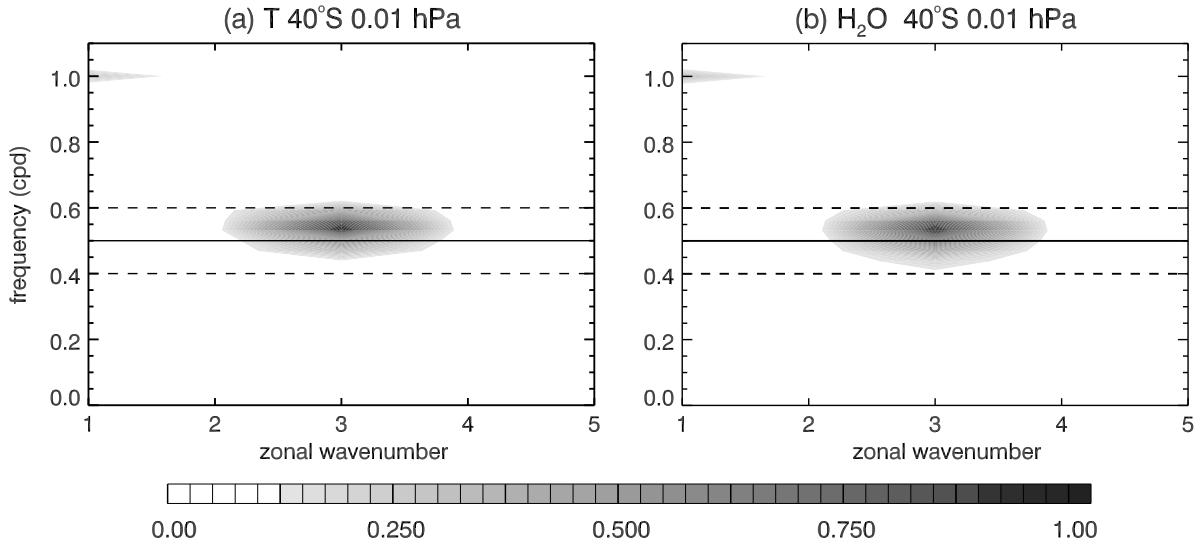

Figure 2. Normalized power spectra derived from NOGAPS-ALPHA (a) temperature and (b) water vapor at 40°S and 0.01 hPa. Dashed horizontal lines enclose the 0.4–0.6 cpd spectral window. The solid horizontal line is drawn at 0.5 cpd. The vertical axis plots westward propagating frequencies only.

Limpasuvan and Wu [2003], which analyzed the Q2DW during January–February 1992 and 1993. Incidentally, the recent study of the Q2DW during January 2006 by *Limpasuvan and Wu* [2009] reported an unusual westward propagating wave number 2 signature in temperature at 90 km and 60°S with a frequency of 0.49 cpd using a linear regression technique that is based on a priori assumptions of spectral characteristics. Spectral analysis of NOGAPS-

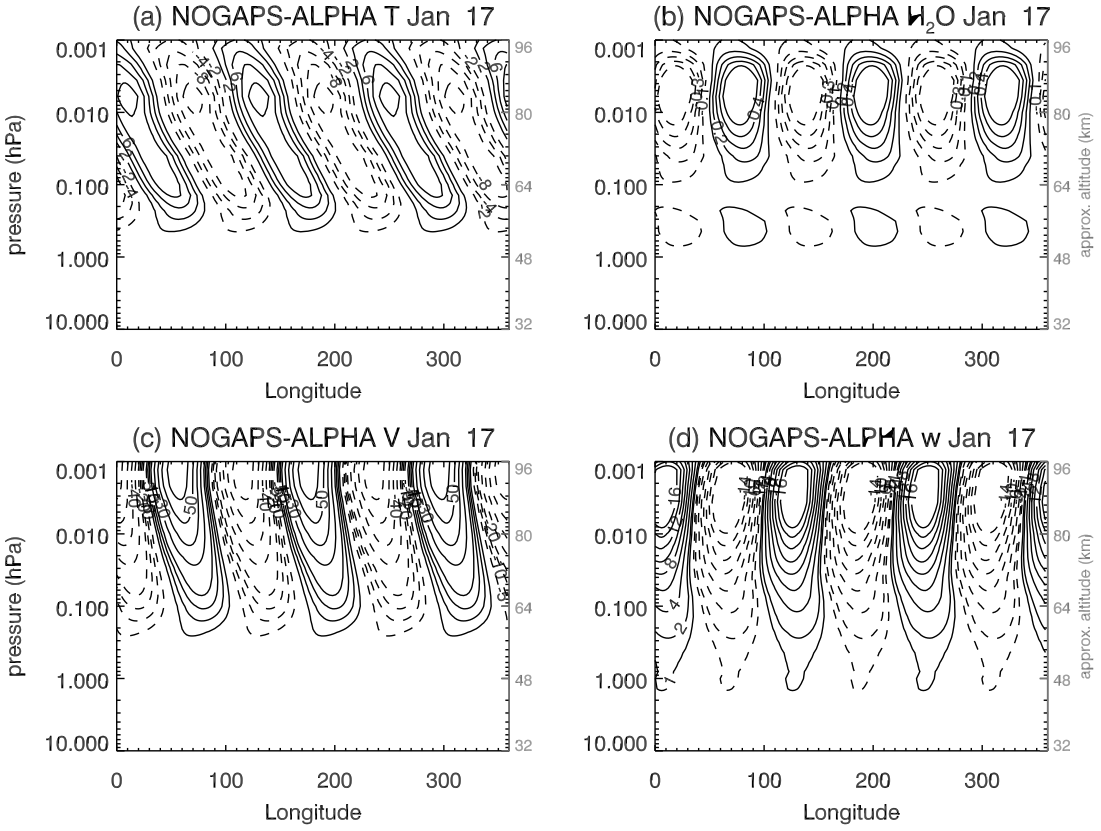

Figure 3. Vertical structure of quasi 2-day wave derived from the filtered NOGAPS-ALPHA analyses at 40°S for 0000 UTC 17 January 2006: (a) temperature, contour interval is 2 K; (b) water vapor, contour interval is 0.1 ppmv; (c) meridional wind, contour interval is 10 m s^{-1}; and (d) vertical velocity, contour interval is 2 cm s^{-1}. Dashed contours denote negative values. Additional meridional wind contours are drawn at ±5 and 15 m s^{-1}; additional vertical velocity contours are drawn at ±1 cm s^{-1}.

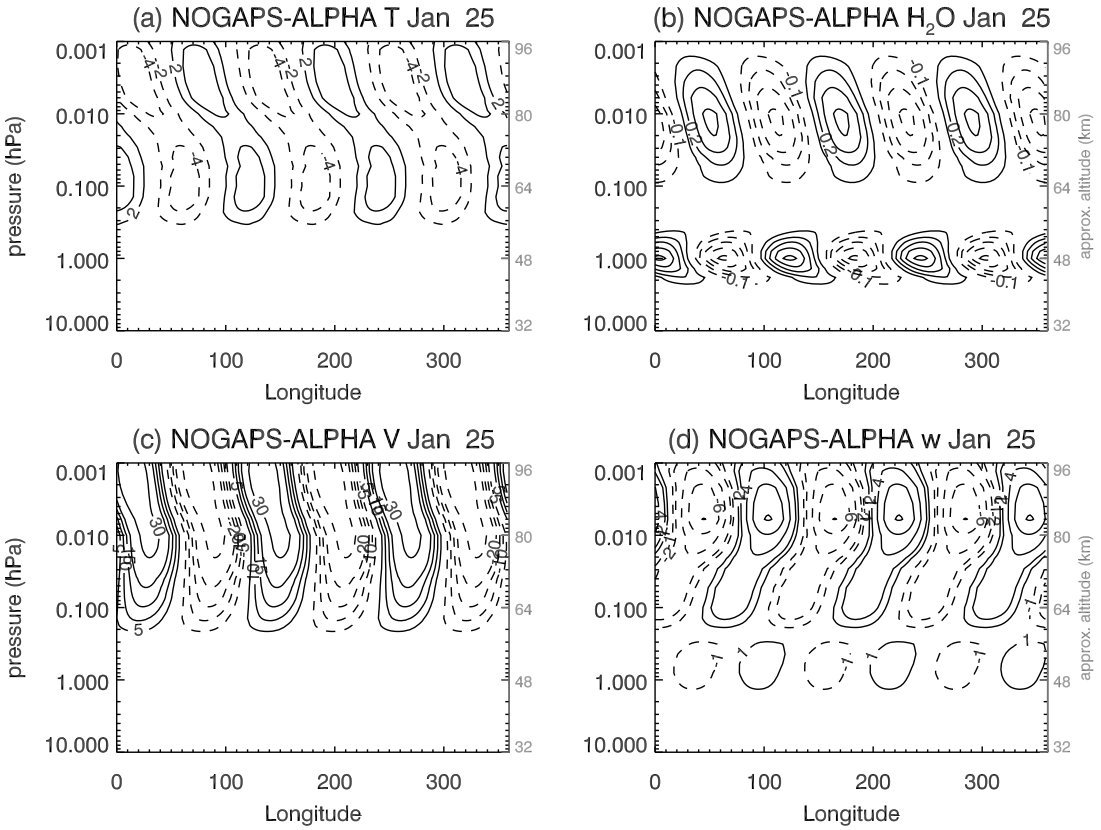

Figure 4. As in Figure 3 but at 20°S for 0000 UTC 25 January 2006.

ALPHA temperatures near 90 km for this time period also finds a sizable wave number 2 component near 60°S, but it is sharply peaked at 0.35 cpd and therefore outside of the 0.4–0.6 cpd window used here for the Q2DW.

4. Results

4.1. January 2006 Mean State

[26] To illustrate the mean atmospheric state during this period, Figure 5 plots NOGAPS-ALPHA zonal mean T, H_2O, v, and u averaged over the 5 January to 5 February 2006 period. A comparison of the winter hemisphere zonal mean temperatures and zonal winds between 10 and 0.1 hPa in Figures 5a and 5d with climatological values from *Randel et al.* [2004] (not shown) shows both warmer temperatures and weaker westerly flow throughout much of this region. In particular, the NOGAPS-ALPHA analyses show a region of mean easterly flow poleward of 50°N (Figure 5d).

[27] The warmer temperatures and absence of strong westerly winds in the winter stratosphere are consistent with the observed breakdown of the polar vortex associated with the SSW on 20 January, as discussed in the study of *Coy et al.* [2008]. Prior to the SSW, there was a high level of planetary wave activity in the extratropical winter lower stratosphere. Figure 6 plots the NOGAPS-ALPHA eddy heat flux ($\overline{v'T'}$) at the 100 hPa level averaged between 25°N and 45°N. We find two distinct periods of high planetary wave activity prior to the SSW. The first period is from 8 to 10 January and the second is from 16 to 20 January.

[28] The zonal mean zonal winds for this period (Figure 5d) also indicate that the summer subtropical easterly jet extends unusually far into the winter hemisphere near the 1 hPa level, almost to 20°N. The peak value of the easterly subtropical jet (<100 m s^{-1}) is also much stronger than normal. Analysis of the zonal wind tendency equation in section 5 finds that the effects of the planetary wave activity leading up to the SSW on 20 January produced unusually strong advection of easterly momentum by the meridional component of the residual circulation.

4.2. General Characteristics of the Q2DW in January 2006

[29] The 2DFFT method described in section 3 was applied to the 6-hourly NOGAPS-ALPHA middle atmospheric analyses from 0000 UTC 5 January 2006 to 1800 UTC 5 February 2006. Time series of the Q2DW were reconstructed from the space-time filtered 2DFFT spectra, and the root-mean-square (RMS) amplitudes were then computed for each day as a function of latitude and pressure. The squared coherency was computed for each set of meteorological variables using the space-time spectra at 40°S and 0.01 hPa as the reference point to which spectra at other latitudes and levels were compared. In almost all cases, coh^2 values met or exceeded the 99% confidence level. The exception is the zonal wind case where values of coh^2 fell below the 99% limit in small, isolated regions in the Northern Hemisphere extratropical stratosphere.

[30] Figure 7 plots the average values of the quasi 2-day wave RMS amplitudes in T, H_2O, v, and vertical velocity (w) over the 5 January to 5 February 2006 period. Peak T amplitudes of 8 K (Figure 7a) are found between 40°S and 50°S near 0.05 and 0.01 hPa. Peak H_2O amplitudes of

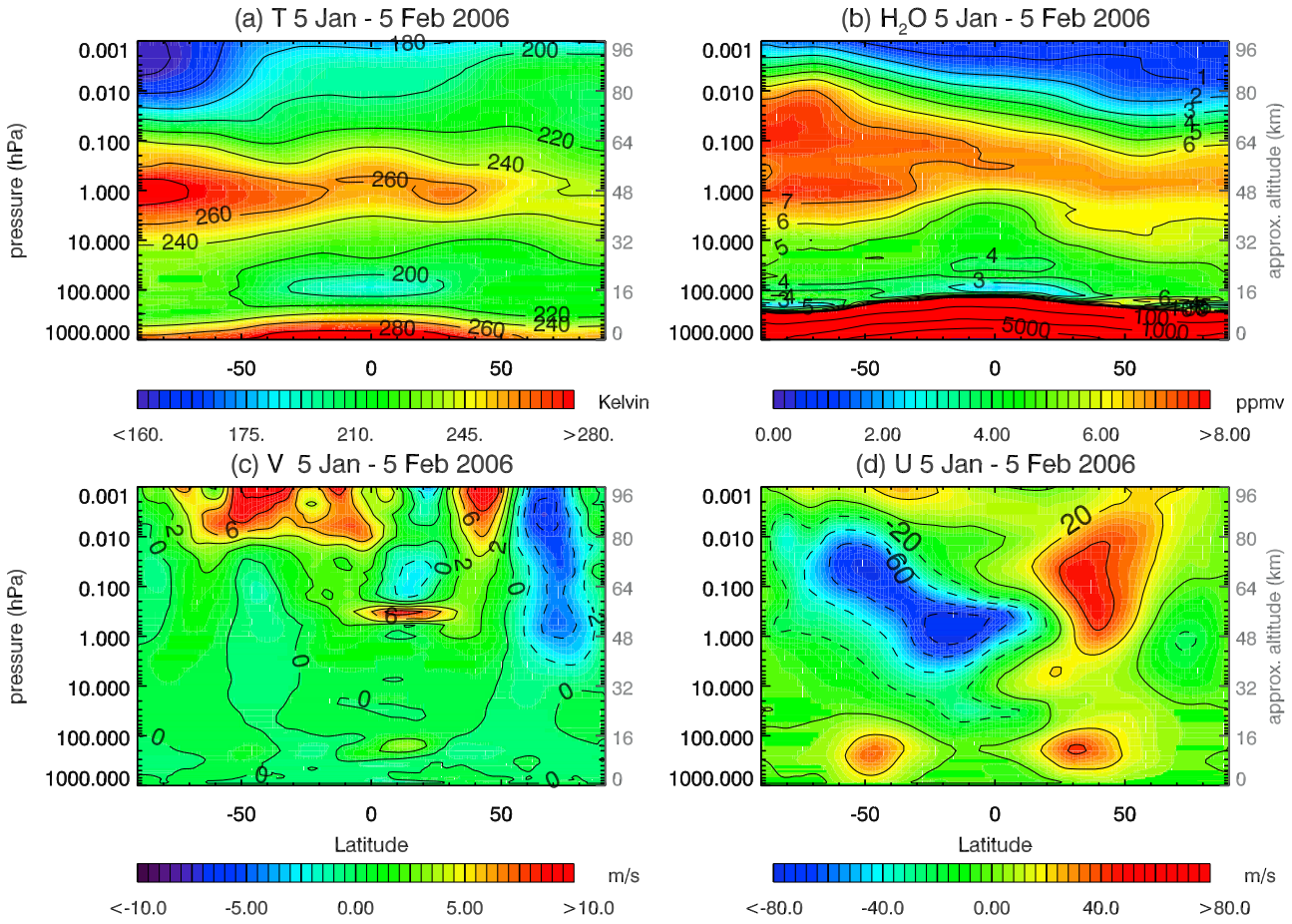

Figure 5. Zonal mean distributions of NOGAPS-ALPHA (a) temperature in Kelvin, (b) water vapor mixing ratio in ppmv, (c) meridional wind in m s^{-1}, and (d) zonal wind in m s^{-1} averaged over the period from 5 January to 5 February 2006.

0.5 ppmv (Figure 7b) occur between 30°S and 50°S near 0.005 hPa. A secondary maximum in H_2O of 0.25 ppmv is found just above the stratopause near 20°S.

[31] The average Q2DW amplitudes in T and H_2O maximize in the summer hemisphere where the gradients in these zonally averaged quantities are largest (see Figures 5a and 5b). As discussed by *Limpasuvan and Wu* [2003], these gradients are maintained by the wave-driven residual meridional circulation. In the stratosphere, this circulation is driven primarily by planetary wave breaking and consists of upward motion over the tropics with poleward and downward motion in the winter extratropics. In the mesosphere, this circulation consists of rising motion over the summer pole, strong meridional flow from summer to winter hemisphere, and downward motion over the winter pole driven by breaking gravity waves. We discuss the impact of the residual circulation derived from the NOGAPS-ALPHA wind and temperature analyses on the evolution of the Q2DW in section 5.

[32] In general, the Q2DW amplitudes in T and H_2O in Figure 7 are in good qualitative and quantitative agreement with the values reported by *Limpasuvan and Wu* [2003] based on UARS MLS measurements for the SH summers of 1992 and 1993. Similar temperature amplitudes were also found in Aura MLS temperatures during late January 2005 [*Limpasuvan et al.*, 2005]. A study of the 2-day wave in SABER temperatures in late January and February of 2002 and 2004 by *Garcia et al.* [2005] found peak amplitudes that were much smaller (~1–3 K) than the values in Figure 7. This discrepancy may be explained by the fact that the Q2DW is strongest just after solstice, whereas the SABER

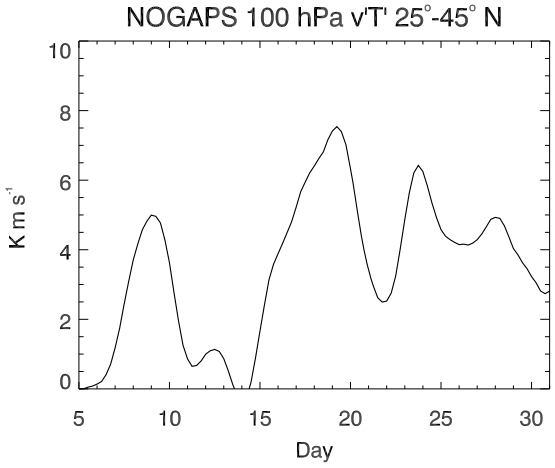

Figure 6. Time series of the eddy heat flux at 100 hPa averaged between 25°N and 45°N over the period 5–31 January 2006 calculated from zonal wave numbers 1–6 in the NOGAPS-ALPHA wind and temperature fields.

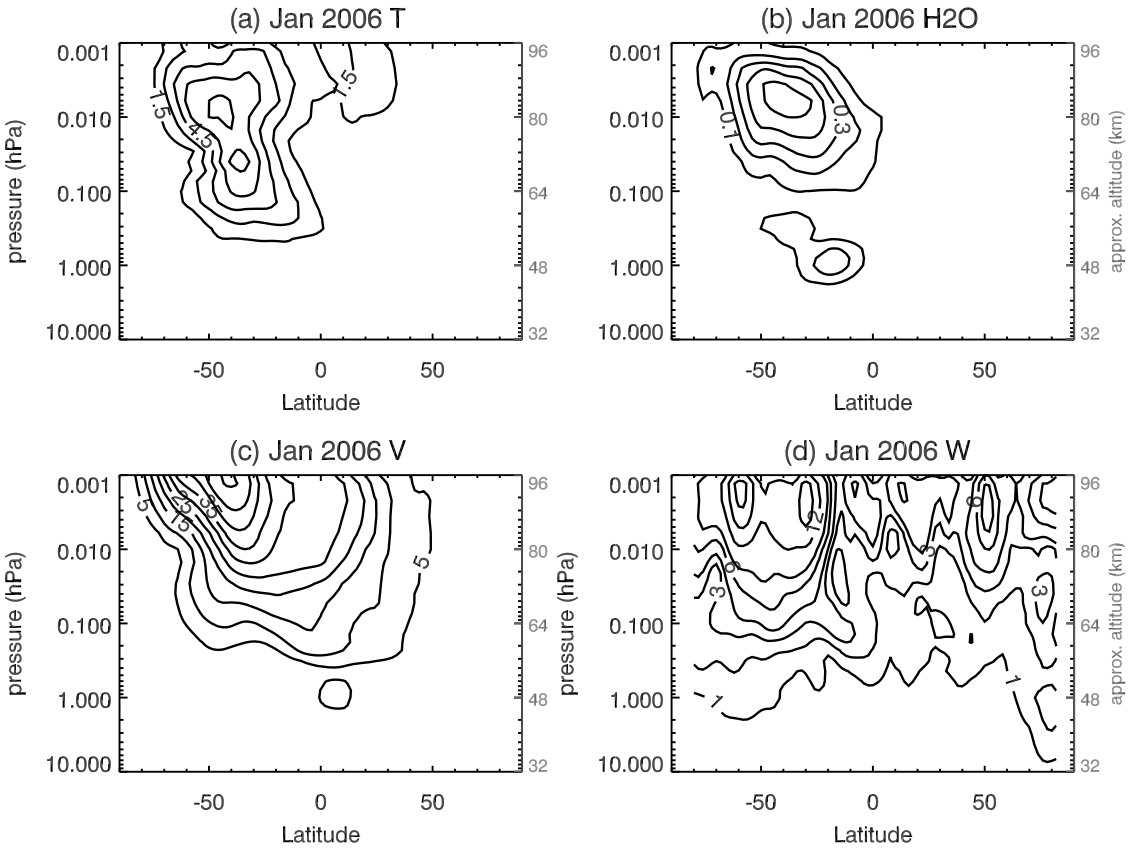

Figure 7. The average quasi 2-day wave RMS amplitude in (a) temperature (Kelvin), (b) water vapor mixing ratio (ppmv), (c) meridional wind (m s^{-1}), and (d) vertical wind (cm s^{-1}) derived from the NOGAPS-ALPHA analyses over the period 5 January to 5 February 2006.

study focused on time periods 1–2 months after summer solstice when the Q2DW is considerably weaker.

[33] While the Q2DW features in T and H_2O are limited mainly to the summer hemisphere, the Q2DW in *v* and *w* (Figures 7c and 7d, respectively) is present in both hemispheres. At the lower levels (0.05–1 hPa), the wave amplitudes exhibit a certain degree of symmetry with respect to latitude, similar to the behavior of a global normal mode. Above the ~0.05 hPa level, the wave amplitudes are sharply peaked in the summer hemisphere. The spatial characteristics of the Q2DW in *v* are similar to those of the fastest growing Rossby gravity wave modes found at solstice in the modeling study of *Salby and Callaghan* [2001, Figure 8]. Overall, these results demonstrate that the NOGAPS-ALPHA analyses provide an accurate and comprehensive description of the Q2DW.

4.3. Temporal Evolution of the Q2DW During January 2006

[34] Next we describe the evolution of the Q2DW during the period from 5 January to 5 February 2006 using reconstructions of the NOGAPS-ALPHA fields from the filtered space-time spectra. We focus on three separate latitude bands where the amplitudes of the Q2DW in T, H_2O, and *v* reach their peak values: 30°S–50°S, 15°S–25°S, and 5°S–5°N. Figure 8 plots the RMS amplitude in the filtered NOGAPS-ALPHA temperatures as a function of time over the three latitude bands. In the extratropical region (Figure 8a), the Q2DW amplitudes peak near 0.05 hPa and 0.5 hPa. Near the 0.05 hPa level, we find the largest Q2DW amplitudes on 10 January and 17 January. Near the 0.05 hPa level, we find peaks on 10 January and from 17 to 25 January. The vertical structure of the temperature Q2DW in the subtropical region (Figure 8b) is qualitatively similar to that seen in the extratropical band (Figure 8a), albeit with smaller amplitudes. The reduced amplitude of the temperature Q2DW in this region is to be expected because the meridional temperature gradients are much smaller in this region. In the equatorial region (Figure 8c), the temperature Q2DW amplitudes are very small, and there is no indication of any vertically coherent structure.

[35] Figure 9 plots the evolution of the Q2DW in NOGAPS-ALPHA H_2O over the three latitude bands during January 2006. In the extratropics (Figure 9a), we find that the largest amplitudes in the upper mesosphere occur near 0.006 hPa. The amplitudes in the H_2O Q2DW at this level peak on 10 and 17 January, similar to the behavior in the extratropical temperature Q2DW (Figure 8a). This double peak is also present in the subtropical region (Figure 9b) between 0.01–0.03 hPa. Interestingly, Figure 9b also shows steadily increasing Q2DW amplitudes in H_2O near the stratopause starting on 15 January and continuing until 26 January. During this period, the vertical structure in the subtropical H_2O Q2DW signal (see Figure 4b) shows the maxima near 1 hPa and 0.01 hPa are 180° out of phase, in contrast to the vertical structure in the extratropical H_2O

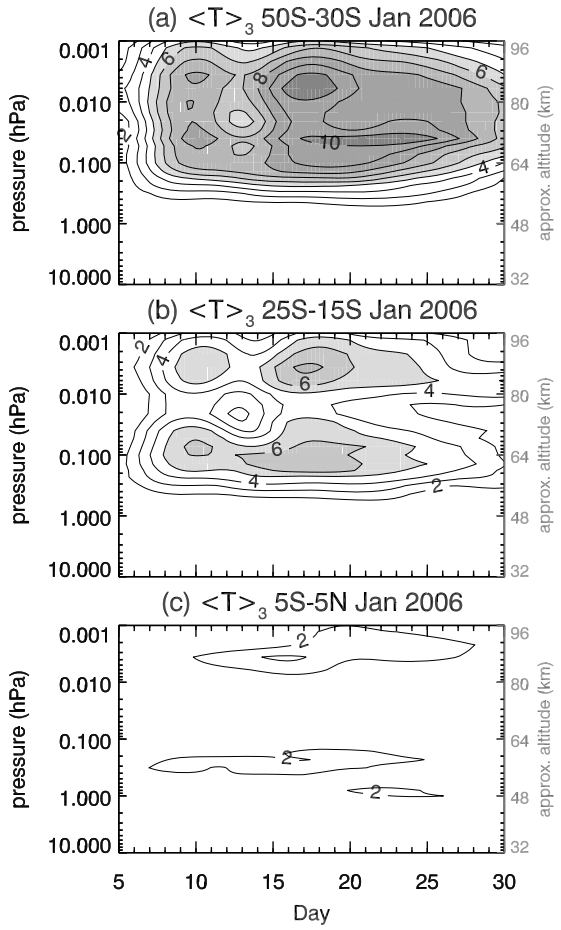

Figure 8. Time variations in the RMS amplitude of the quasi 2-day wave in NOGAPS-ALPHA temperature for the period 5–31 January 2006 averaged over the latitude bands (a) 50°S–30°S, (b) 25°S–15°S, and (c) 5°S–5°N. Contour interval is 1 K.

Q2DW (Figure 3b). Over the equator, Figure 9c shows a negligible Q2DW signal in H_2O.

[36] The time behavior of the Q2DW meridional wind during January 2006 is plotted in Figure 10. In both the extratropical and subtropical regions, Figures 10a and 10b, respectively, we again find a vertically coherent double peak structure that is remarkably similar to the patterns in the T and H_2O Q2DW amplitudes between 0.1 and 0.001 hPa. Over the equator (Figure 10c), the same double peak structure is also present above the 0.1 hPa level. In addition, the Q2DW in *v* over the equator shows a distinct minimum near 0.3 hPa. Near the stratopause, the Q2DW in *v* increases again with distinct peaks on 10, 20, and 26 January. As we discuss in section 4.4, the localized minimum in meridional wind Q2DW amplitudes near the 0.3 hPa level coincides with the presence of inertially unstable circulations in the lower equatorial mesosphere.

[37] The evolution of the Q2DW in vertical velocity, *w*, which is derived from the divergence of the space-time filtered NOGAPS-ALPHA horizontal winds (*u* and *v*) is plotted in Figure 11. The same double peak structure is evident in the extratropical upper mesosphere (Figure 11a). In the subtropical region (Figure 11b), the amplitude of the Q2DW in *w* peaks near 0.002 hPa on 17 January. Near the subtropical stratopause, Figure 11b shows that the Q2DW amplitude in *w* peaks on 25 January. This is the same time when the Q2DW in H_2O in this region increases (see Figure 9b). The vertical structure of the Q2DW in *w* at 20°S (Figure 4d) indicates a phase shift between 1 hPa and 0.01 hPa that is remarkably similar to that seen in the subtropical Q2DW in H_2O (Figure 4b). Over the equator (Figure 11c), the Q2DW in *w* is largest between 0.01 and 0.001 hPa and is quite small near the stratopause.

[38] Overall, a generally consistent picture of the Q2DW emerges from the NOGAPS-ALPHA analyses. In the extratropical summer mesosphere, the Q2DW in *v* is accompanied by a response in both T and H_2O in regions where strong meridional gradients in these quantities exist. However, we find a sizable Q2DW signal in H_2O near the stratopause during late January, in the absence of a strong Q2DW in *v* (Figure 9b). Based on the similarities in the amplitude and phase of the Q2DW signals in H_2O and *w*, it appears that vertical motions associated with the Q2DW (Figure 11b) superimposed on the vertical gradient in H_2O are driving the Q2DW in H_2O near 1 hPa. The study of *Limpasuvan and Wu* [2003] found a similar Q2DW signal in H_2O near 1 hPa during January–February 1992 when a series of SSWs took place, but not in the following year when SSWs were absent.

[39] While the episodic nature of the Q2DW has been noted in earlier studies, the NOGAPS-ALPHA analyses

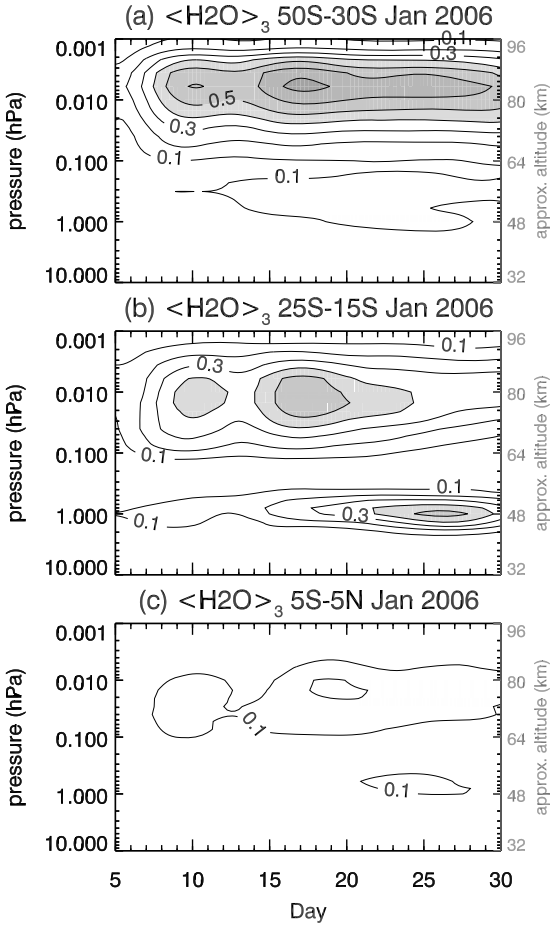

Figure 9. As in Figure 8 but for NOGAPS-ALPHA water vapor mixing ratios. Contour interval is 0.1 ppmv.

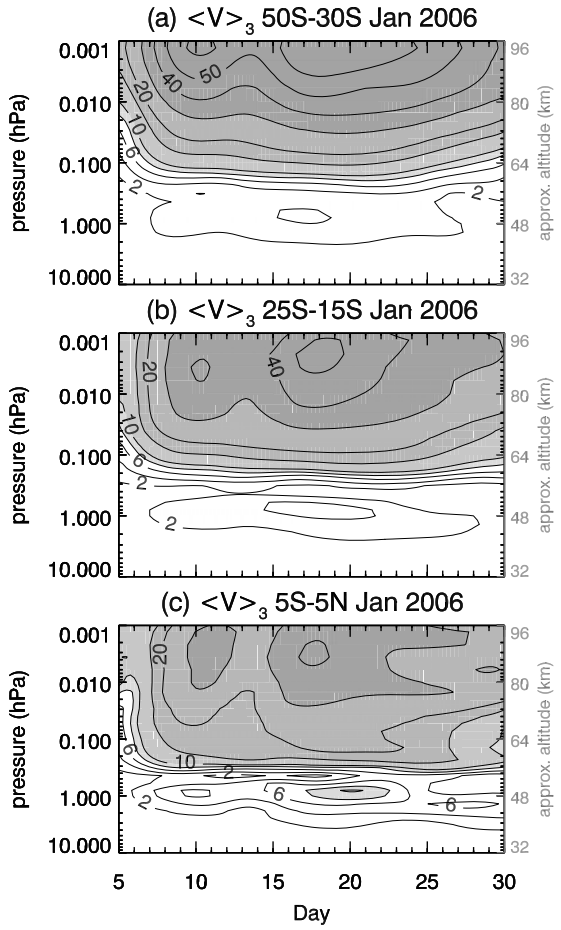

Figure 10. As in Figure 8 but for NOGAPS-ALPHA meridional wind (in m/s). Contours are drawn at 2, 4, 6, 8, 10, 15, 20, 30, 40, 50, and 60 m s^{-1}.

show here for the first time that there is a generally coherent vertical structure to these episodic variations throughout upper mesosphere (i.e., 0.1–0.001 hPa). The similar time behavior of the meridional wind Q2DW in this altitude region throughout all three latitude bands suggests that the evolution of the Q2DW is affected by a common, large-scale process. Section 4.4 presents diagnostic calculations based on the global synoptic NOGAPS-ALPHA analyses to identify the sources of the 2-day forcing in each of these regions. Our results show that the strong planetary wave forcing in the winter extratropical stratosphere leading up to the SSW on 20 January 2006 played a significant role in modulating the Q2DW throughout the middle atmosphere.

4.4. Inertial Instability, Planetary Waves, and the Q2DW

[40] As noted in section 1, previous studies have linked Q2DW activity in the subtropical stratopause region with planetary wave activity in the subtropical winter stratosphere through the presence of inertially unstable circulations in the equatorial lower mesosphere [*Orsolini et al.*, 1997; *Limpasuvan et al.*, 2000a]. This section briefly summarizes this link and presents evidence that inertial instability influenced the evolution of the Q2DW during January 2006.

[41] The zonal mean circulation can be considered inertially unstable if the quantity $f^2(1 - Ri^{-1}) - f\overline{u}_\phi < 0$, where f is the Coriolis parameter, Ri is the Richardson number, and the subscript ϕ indicates a derivative with respect to latitude [*Andrews et al.*, 1987]. This relation is commonly approximated as $f\,(f - \overline{u}_\phi) < 0$, which holds for barotropic flow (i.e., $Ri \gg 1$). However, NOGAPS-ALPHA zonal wind fields indicate that values of $Ri \approx 3$ are common between 0.1 and 0.3 hPa within 10° of the equator. To avoid any possible errors in identifying inertially unstable regions in the analyses, we use the full expression for the inertially unstable criterion.

[42] The observational study of *Hitchman et al.* [1987] showed that the penetration of planetary wave number 1 and 2 disturbances into the Northern subtropics triggers inertially unstable circulations in the equatorial lower mesosphere that produce a characteristic "pancake" structure in the temperature. The modeling study of *Sassi et al.* [1993] also demonstrated that inertially unstable circulations form in response to planetary wave forcing in the midlatitude winter stratosphere. The redistribution of momentum by the inertially unstable circulations produces strong advection of summer easterlies into the winter hemisphere over a vertically shallow region above the tropical stratopause. This advection strengthens the meridional curvature in the zonal

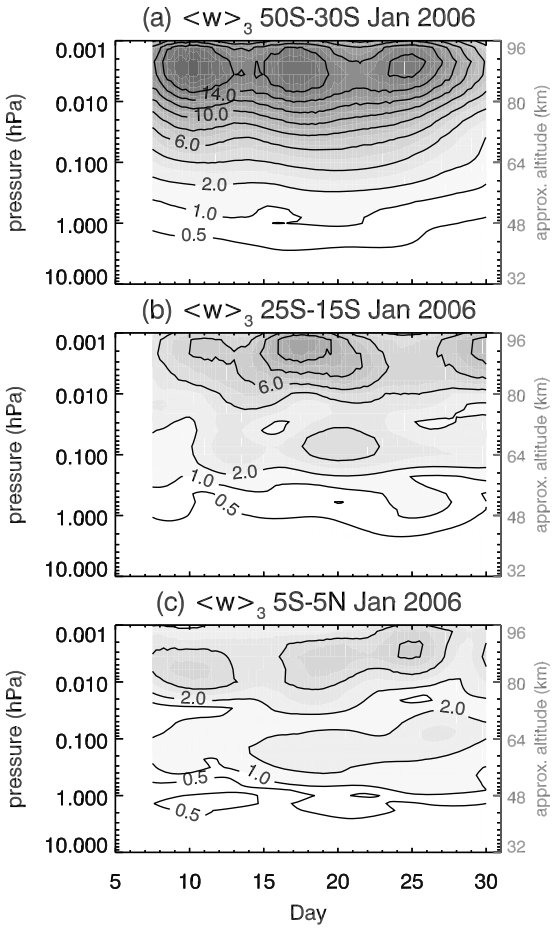

Figure 11. As in Figure 8 but for NOGAPS-ALPHA vertical velocity. Contour interval is 2 cm s^{-1} with additional contours drawn at 0.5 and 1 cm s^{-1}.

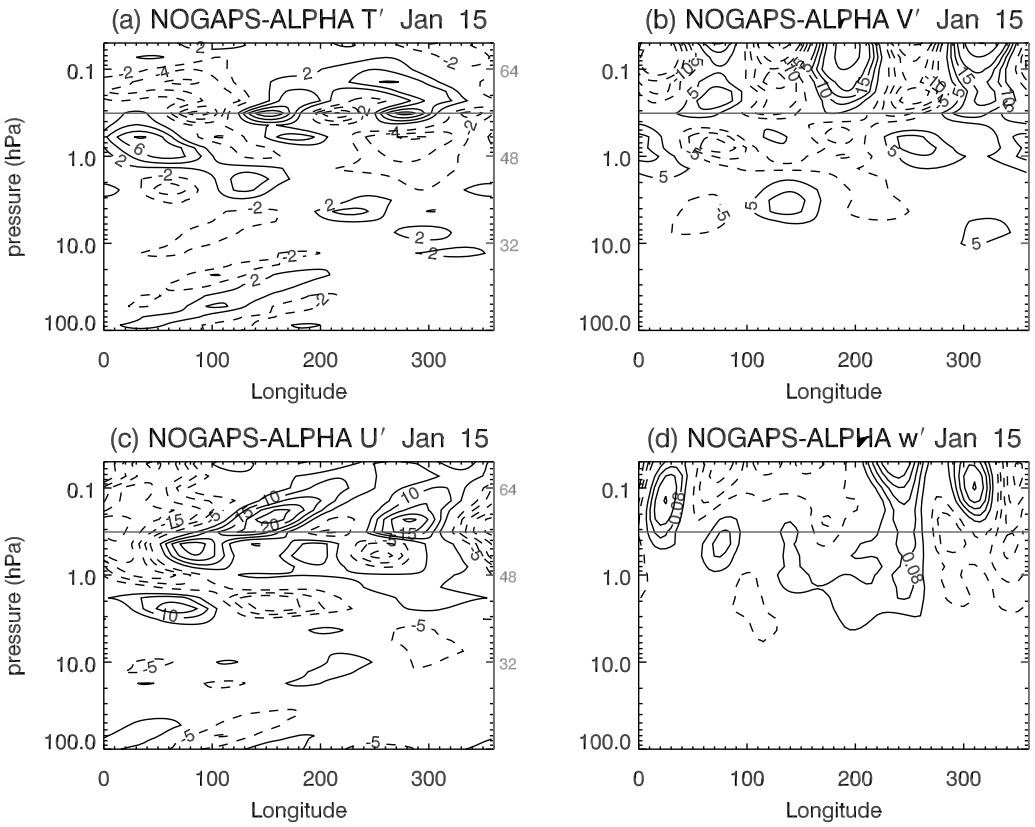

Figure 12. Longitude-pressure cross sections of the zonally asymmetric component in (a) temperature, (b) meridional wind, (c) zonal wind, and (d) vertical wind daily averaged between 5°S and 5°N computed from zonal wave numbers 1–6 of the filtered NOGAPS-ALPHA analyses for 15 January 2006. Horizontal line indicates 0.32 hPa level.

winds, which favors the formation of barotropic instabilities [*Orsolini et al.*, 1997]. The study of *Limpasuvan et al.* [2000a] showed that the barotropic instabilities formed in response to the inertial circulations provide forcing of the quasi 2-day wave near the tropical stratopause.

[43] The NOGAPS-ALPHA horizontal wind and temperature fields indicate that inertially unstable circulations were present during the period of strong planetary wave activity prior to the SSW on 20 January 2006. For example, Figure 12 plots daily averaged vertical cross sections of the zonally asymmetric components T′, u', and v' on 15 January 2006 averaged between 5°S and 5°N obtained from zonal wave numbers 1–6 of the spatially filtered NOGAPS-ALPHA analyses. No time filtering is performed, so both propagating and stationary modes are included in the vertical cross sections. The temperature cross section on this day reveals a stationary zonal wave number 3 structure with limited vertical extent centered near the 0.3 hPa level indicative of the "pancake" structures related to inertial instability described in the study of *Hitchman et al.* [1987]. Also plotted in Figure 12 are the corresponding cross sections of meridional, zonal, and vertical velocity anomalies. The latter are derived from the filtered horizontal divergence fields based on integration of the continuity equation. Figure 12 shows that the circulation patterns associated with the "pancake" structure in temperature extend both above and below the 0.3 hPa level in agreement with the circulation patterns associated with inertial instability [see, e.g., *Hitchman et al.*, 1987, Figure 8].

[44] To show how the inertially unstable circulations in the equatorial mesosphere evolve over the January 2006 period in relation to planetary wave activity in the winter stratosphere, Figure 13 compares daily variations in RMS amplitude of the zonal wave number 3 component in T′ over the 5°S–5°N latitude band with daily variations in the RMS amplitude of zonal waves 1–2 in T′ over the 15°N–30°N latitude band. The highly localized peaks in the wave 3 temperature amplitudes between 0.3–0.5 hPa on 8 January and 13–15 January (Figure 13a) indicate when inertially unstable circulations in the equatorial lower mesosphere are strongest. The timing of these peaks relative to the peaks in the amplitude of waves 1 and 2 in the subtropics near 2–3 hPa (Figure 13b) indicates that the strong planetary wave activity on 8–10 January likely produced the inertially unstable circulation features.

[45] In addition to the inertial instabilities, the wave 3 temperature amplitudes over the equator in Figure 13a also capture the elements of the Q2DW near 1 hPa around 20 January that were seen in the space-time filtered temperature fields (Figure 8c). The appearance of the Q2DW signal 5–10 days after the peak in the inertially unstable circulation feature raises the possibility that the inertial instabilities themselves are a source of wave 3 forcing for the Q2DW. As we show in section 4.5, diagnostic calcula-

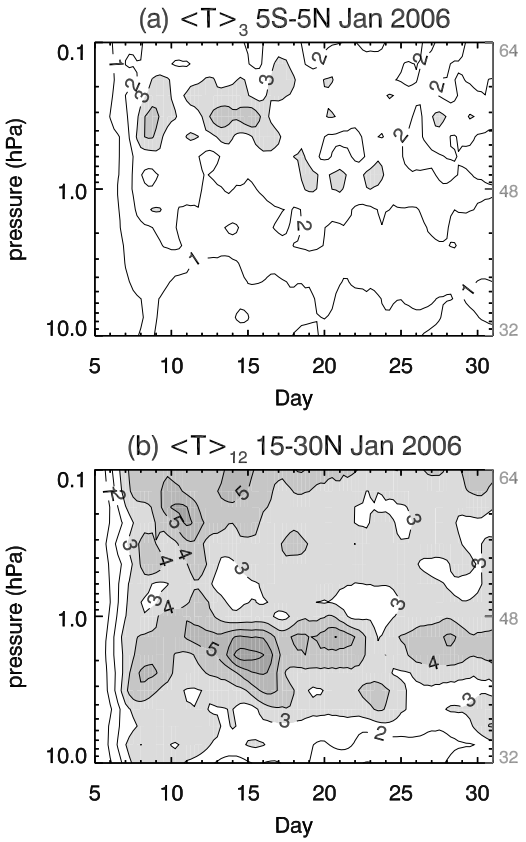

Figure 13. Pressure-time cross sections of the daily averaged RMS amplitude in spatially filtered NOGAPS-ALPHA temperature during 5–31 January 2006: (a) zonal wave number 3 averaged between 5°S and 5°N and (b) zonal wave numbers 1–2 averaged between 15°N and 30°N.

tions of eddy heat and momentum fluxes based on the NOGAPS-ALPHA analyses indicate that the inertial instabilities in the equatorial lower mesosphere are not a source of Q2DW forcing per se. Instead, they modulate the barotropically unstable sources of Q2DW forcing through cross-equatorial advection of easterly momentum from summer to winter hemisphere.

4.5. Diagnostic Calculations of Q2DW Forcing

[46] This section presents diagnostic calculations of the Q2DW forcing based on eddy heat and momentum fluxes derived from the space-time filtered NOGAPS-ALPHA analyses. These calculations are used to characterize the physical processes affecting the evolution of the Q2DW amplitudes seen over the January 2006 period in Figures 8–11.

[47] In general, wave forcing of the zonal mean background state can be described in terms of the Eliassen-Palm (EP) flux vector **F** where

$$\mathbf{F} = \left[F_\phi, F_z\right] = \rho a \cos\phi \cdot \left[-\overline{u'v'} - \left(\frac{R}{HN^2}\,\overline{u}_z\overline{v'T'}\right), \left(f - \frac{1}{a\cos\phi}\left[\overline{u}\cos\phi\right]_\phi\right)\frac{R}{HN^2}\overline{v'T'} - \overline{u'w'}\right]. \tag{3}$$

Here ρ is density, a is the radius of the Earth, ϕ is latitude, z is the log-pressure vertical coordinate, R is the gas constant, N is the Brundt-Vaisala frequency, and f is the Coriolis parameter. The EP flux vector can be regarded as the combination of the effects of large-scale planetary waves $\mathbf{F_p}$ and smaller-scale gravity waves $\mathbf{F_g}$ where

$$\mathbf{F_p}[\phi, z] = \rho a \cos\phi\left[-\overline{u'v'}, \left(f - \frac{1}{a\cos\phi}\left[\overline{u}\cos\phi\right]_\phi\right)\frac{R}{HN^2}\overline{v'T'}\right] \tag{4}$$

$$\mathbf{F_g}[z] = \rho a \cos\phi\left[-\overline{u'w'}\right], \tag{5}$$

where the meridional component of $\mathbf{F_p}$ is proportional to the eddy momentum flux $\overline{u'v'}$, the vertical component of $\mathbf{F_p}$ is proportional to the eddy heat flux $\overline{v'T'}$, and the vertical component of $\mathbf{F_g}$ is proportional to the vertical eddy momentum flux $\overline{w'u'}$.

[48] The study of *Lieberman* [1999, 2002] showed that EP flux calculations based on space-time filtered dynamical fields can characterize both the sources and propagation of the 2-day wave forcing. To diagnose the sources of the Q2DW activity seen in the NOGAPS-ALPHA analyses, we have computed the eddy heat and momentum fluxes and the corresponding EP fluxes from daily averages of the space-time filtered NOGAPS-ALPHA u, v, w, and T fields for days 5–31 of January 2006.

[49] Figure 14 plots the daily averaged (unfiltered) zonal mean zonal winds on 10, 15, 20, and 25 January. These days were chosen to capture the peaks in the Q2DW amplitudes seen in Figures 8–11. EP fluxes for each day were computed from daily averages of the space-time filtered horizontal wind and temperature fields with the same spectral filter used to isolate the Q2DW in the analyses (i.e., zonal wave number 3 and 0.4–0.6 cpd). In Figure 14, the resulting EP flux vectors are superimposed on the background zonal wind fields for each day. These vectors represent the planetary wave component of the EP flux $\mathbf{F_p}$.

[50] As Figure 14 shows, January 2006 was an unusual period in that the zonal mean zonal winds in the winter extratropics are either weakly westerly or easterly throughout the month owing to the strong planetary wave activity leading up to the SSW on 20 January. During this period, the summer easterly jet has two local maxima: In the lower mesosphere near 20°S, and in the upper mesosphere near 50°S. The lower mesospheric branch reaches its maximum intensity (>100 m s^{-1}) and extends farthest north on 15 January.

[51] Also plotted in Figure 14 is the location where the background zonal wind matches the Q2DW phase speed (red contour). The phase speed is determined from the ratio of zonal wave number and frequency using values of 3 and 0.525 cpd, respectively. These values correspond to the peak in the NOGAPS-ALPHA T power spectrum in Figure 2. The equivalent period at the spectral peak is 1.9 days, and so we will refer to this wave mode as the (3, 1.9) mode. The quasi-geostrophic potential vorticity ($\overline{q}$) is also calculated from the unfiltered NOGAPS-ALPHA wind and temperature fields. Baroclinic or barotropic instabilities can grow in regions where the meridional gradient in $\overline{q}$ is negative (i.e., $\overline{q}_\phi < 0$), as indicated by the shading in Figure 14.

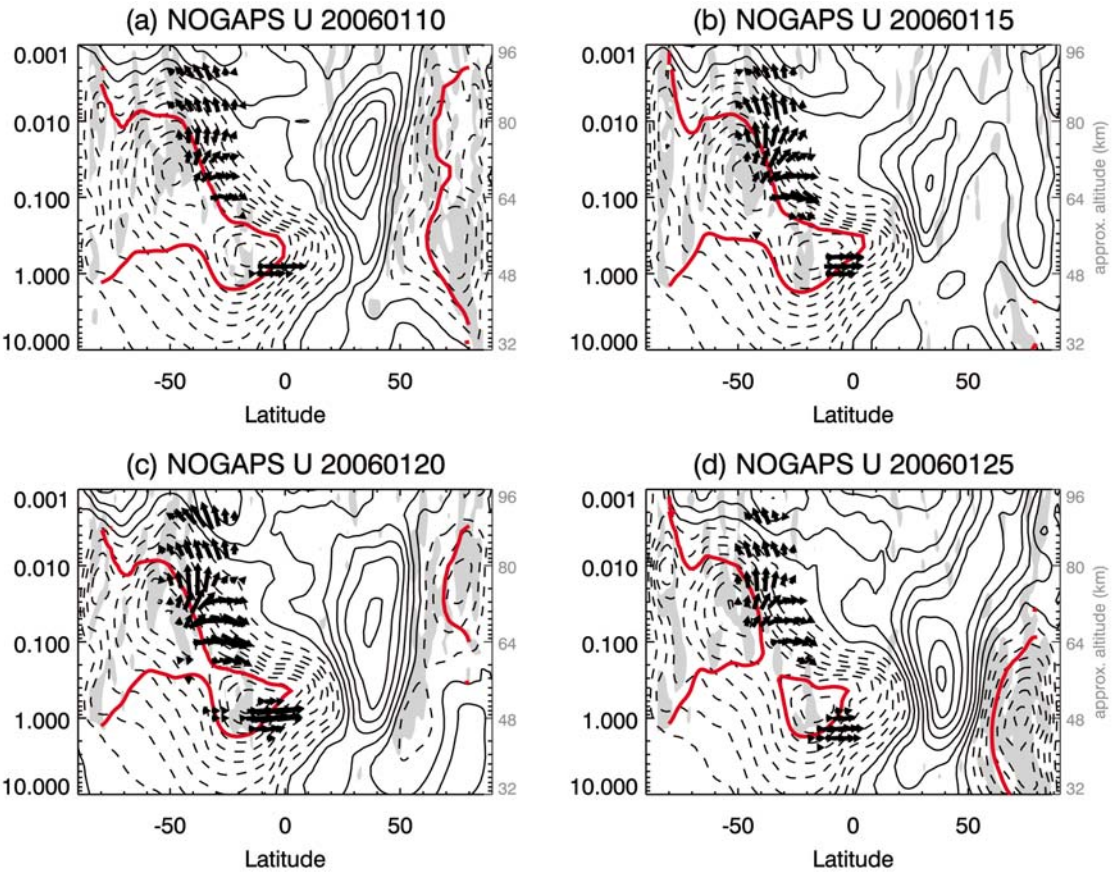

Figure 14. Daily average values of unfiltered zonal mean zonal winds and EP flux vectors associated with the quasi 2-day wave computed from space-time filtered NOGAPS-ALPHA wind and temperature fields on (a) 10 January, (b) 15 January, (c) 20 January, and (d) 25 January 2006. Positive (negative) zonal wind values are plotted with solid (dashed) contours. The contour interval is 10 m s^{-1}. Also plotted are corresponding EP flux vectors associated with the quasi 2-day wave computed from the filtered wind and temperature fields. Shading indicates regions where $\overline{q}_\phi < 0$. The red curve denotes the location of the zonal wave number (3, 1.9) cpd critical line.

[52] Figure 14 shows two distinct regions where the EP flux vectors originate. The first region is located between 30°S and 50°S and between 0.1 and 0.01 hPa, where strong curvature of the zonal wind profile produces regions of $\overline{q}_\phi < 0$ along the equatorward flank of the summer easterly jet. The second region is located just above the stratopause near 10°S, where strong meridional gradients in zonal wind and negative regions of $\overline{q}_\phi$ exist. In both regions, the EP flux vectors point away from the Q2DW phase speed contour, indicating propagation away from a critical line. We note that these two regions are separated by a "null" region between the 0.3 and 0.5 hPa levels where the EP fluxes are negligible.

[53] Additional EP flux diagnostics computed from the NOGAPS-ALPHA horizontal winds and temperatures that have been spatially filtered to isolate zonal wave number 3 while preserving all eastward and westward propagating modes (not shown) are remarkably similar to those in Figure 14 in that they also indicate a region of negligible EP flux between 0.3 and 0.6 hPa, where inertially unstable circulations were found (see Figure 12). Thus we find no evidence for zonal wave number 3 disturbances in this null region directly forcing the global 2-day wave mode. Instead, the main role of the inertially unstable circulations in this region appears to be maintaining barotropic instabilities in the zonal wind profile over the equator that serve as a source of Q2DW forcing, in agreement with earlier studies [*Orsolini et al.*, 1997; *Limpasuvan et al.*, 2000b].

[54] The EP flux vectors in the extratropical source region (Figure 14) are predominantly upward, denoting strong eddy heat flux ($\overline{v'T'}$) that is indicative of baroclinic instability. The magnitudes of the EP flux vectors in the extratropical source region maximize on 15 and 20 January, consistent with the timing of the peak Q2DW amplitudes in, for example, Figure 8. In contrast, the EP flux vectors associated with Q2DW wave activity in the tropical source region near 1 hPa are almost entirely equatorward, indicating strong eddy momentum flux ($\overline{u'v'}$) that characterizes barotropic instability. The meridional component of the Q2DW EP flux vectors near 1 hPa shows a dramatic increase on 20 January. This coincides with the peak Q2DW amplitude in v near 1 hPa seen in Figure 12c, and occurs at the same time as the stratospheric warming in the winter hemisphere.

[55] The similar time behavior of the Q2DW amplitudes at different latitude and altitude regions shown in section 4.4 suggests that the Q2DW forcing could be controlled by a

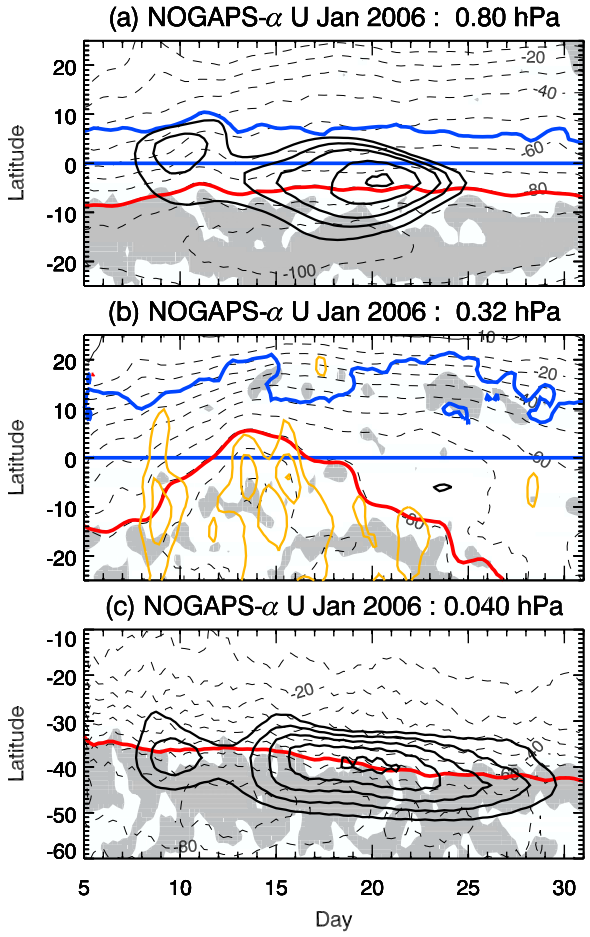

Figure 15. Time-latitude plots of unfiltered NOGAPS-ALPHA zonal mean zonal wind at (a) 0.8 hPa, (b) 0.32 hPa, and (c) 0.04 hPa. Thick black contours in Figures 15a and 15c denote peak values of the quasi 2-day wave eddy momentum flux and eddy heat flux, respectively. Thick orange contours in Figure 15b denote peak RMS amplitude in zonal wave 3 temperature over the equator. Shaded regions indicate where $\overline{q}_\phi < 0$. Thick red curves denote the critical line for the (3, 1.9) mode. Thick blue curves enclose inertially unstable regions.

common factor, despite the different nature of the forcing in each region (i.e., baroclinic forcing in the extratropics versus barotropic forcing near the equator). To better illustrate the time behavior of the wave forcing associated with the Q2DW, Figure 15 compares the eddy heat and momentum fluxes derived from the filtered wind and temperature fields for 5–31 January 2006 with variations in the zonal mean zonal wind within each of the three regions identified above: The tropical source region, the null region, and the extratropical source region.

[56] Figure 15a plots the daily variations in Q2DW eddy momentum fluxes and in the unfiltered zonal mean zonal winds over the tropics at the 0.8 hPa level. Also plotted are the locations of the (3, 1.9) critical line (red curve), the region of inertial instability (blue curves), and regions where $\overline{q}_\phi < 0$ (shading). Peak values of the eddy momentum flux $\overline{u'v'}$ occur equatorward of the critical line for the (3, 1.9) mode near the regions of instability ($\overline{q}_\phi < 0$). The peak eddy momentum flux at 0.8 hPa appears to shift from the inertially unstable region near 5°N on 10 January southward toward the location of the (3, 1.9) critical line (and the region of $\overline{q}_\phi < 0$) by 20 January. This suggests that both inertial instability and barotropic instability are affecting the time behavior of the Q2DW in the tropical source region.

[57] Figure 15b plots the zonal wind variations within the "null" region at 0.32 hPa. The lack of significant eddy heat or momentum fluxes associated with the Q2DW in the null region is to be expected since the background flow at this level is quite stable, as indicated by the limited regions where $\overline{q}_\phi < 0$ in Figure 15b. However, the zonal winds at this level indicate a "bulge" of very strong easterly flow developing between 10 and 15 January extending across the equator. This equatorward bulge in the zonal wind profile at 0.32 hPa is preceded by a maxima in RMS zonal wave 3 temperature amplitude (thick orange contours) on 10 January and coincides with the extension of the 2-day wave critical line across the equator into the inertially unstable region. Subsequently, the inertially unstable region contracts between 15 and 20 January and the easterly jet maximum diminishes rapidly. This sequence of events indicates that inertially unstable circulations are modifying the momentum distribution in the equatorial lower mesosphere [*Hitchman et al.*, 1987].

[58] Figure 15c plots the daily variations in Q2DW eddy heat fluxes and zonal mean zonal wind in the extratropical source region at 0.04 hPa. The timing of the peak eddy heat fluxes shown in Figure 15c is similar to the timing of the eddy momentum fluxes in the tropical source region (Figure 15a). For example, there is an initial peak centered on 10 January followed by a steady increase from 15 to 20 January. In addition, the eddy heat and momentum fluxes within the two regions both peak on 20 January, coincident with the stratospheric warming. The peak eddy heat flux at 0.04 hPa remains in close proximity to the (3, 1.9) critical line throughout the month, indicating that baroclinic instability along the equatorward flank of the extratropical easterly jet is the main source of Q2DW forcing in the extratropical source region.

[59] The diagnostic calculations presented in this section indicate that the Q2DW forcing in the summer extratropical upper mesosphere is related primarily to baroclinic instability along the equatorward flank of the easterly jet. In contrast, the Q2DW forcing near the stratopause is related primarily to barotropic instability produced by the unusually strong easterly flow extending across the equator into the winter hemisphere. In between the two regions lies a null region where no Q2DW forcing occurs. While not acting as a direct source of Q2DW forcing, inertial instability in this null region appears to be modifying the zonal mean zonal winds near the equator. The Q2DW eddy heat and momentum fluxes within the extratropical and tropical source regions, respectively, exhibit similar time behavior. In section 5, we discuss how planetary wave activity in the winter hemisphere leading up to the 20 January SSW may have modified the zonal winds, and thus the Q2DW forcing, within these two regions.

5. Discussion

[60] As stated in section 1, earlier studies have linked Q2DW forcing near the stratopause with planetary wave

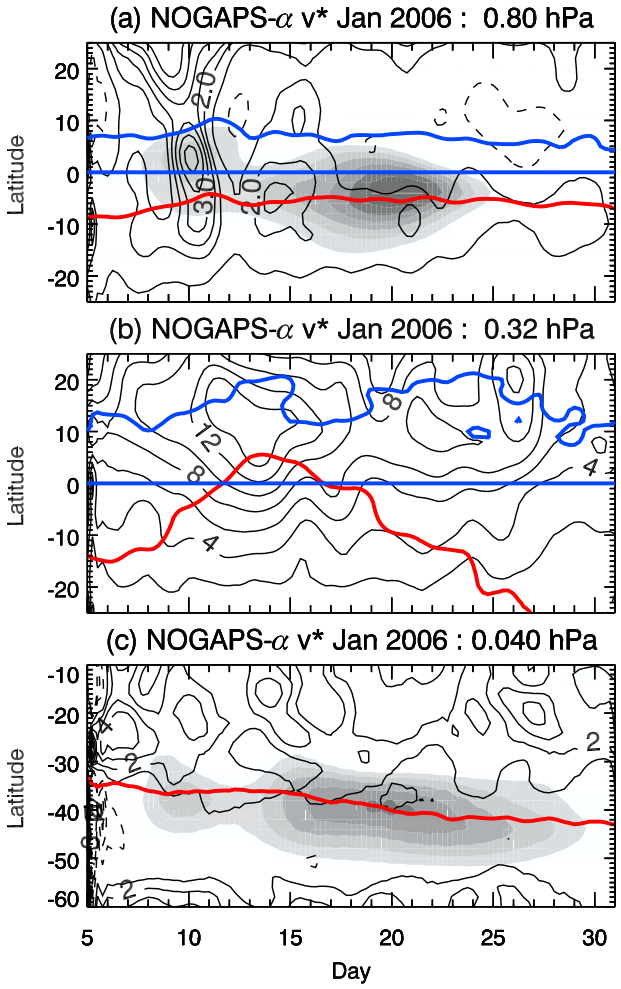

Figure 16. The meridional component of the residual circulation $\overline{v}^*$ (solid contours, in m s^{-1}) at (a) 0.8 hPa, (b) 0.32 hPa, and (c) 0.04 hPa from 5 to 31 January 2006 derived from low-pass waves 1 and 2 filtered NOGAPS-ALPHA horizontal wind and temperature fields. Shading denotes the quasi 2-day wave eddy heat/momentum fluxes from Figure 15. Thick red and blue curves denote the locations of the (3, 1.9) critical line and of inertially unstable regions, respectively.

activity in the winter stratosphere through the formation of inertially unstable circulations in the equatorial lower mesosphere. However, possible links between planetary wave activity in the winter stratosphere and the extratropical Q2DW source region are not as well established. One possible explanation was raised in the modeling study of *Salby and Callaghan* [2003], which suggested that planetary wave activity in the winter hemisphere could alter the residual meridional circulation and, by extension, summer mesospheric easterly winds through changes in the Coriolis torque. However, the magnitude and spatial extent of such an effect is not clear. Breaking gravity waves in the summertime upper mesosphere are known to produce the vertical wind shears that support baroclinic instability in the extratropical source region of the Q2DW. Thus it is possible that any zonal wind anomalies in the summer hemisphere related to the SSW in the winter stratosphere could also impact the extratropical source region through preferential filtering of upward propagating gravity waves.

[61] To better characterize these processes, we examine the relationship between planetary wave activity in the NH stratosphere, the residual circulation, and the momentum budget in both the tropical and extratropical Q2DW source regions during January 2006 using NOGAPS-ALPHA meteorological fields. We do so by evaluating the individual terms in the zonal wind tendency equation using the Transformed Eulerian Mean (TEM) formulation [see, e.g., *Andrews et al.*, 1987], where

$$\frac{\partial \overline{u}}{\partial t} + (a\cos\phi)^{-1}\frac{\partial}{\partial \phi}(\overline{u}\cos\phi)\overline{v}^* - f\overline{v}^* + \frac{\partial \overline{u}}{\partial z}\overline{w}^* = \frac{1}{\rho}\left(\nabla\cdot\mathbf{F_p} + \nabla\cdot\mathbf{F_g}\right) + \overline{X}. \quad (6)$$

Here $\overline{v}^*$ and $\overline{w}^*$ represent the meridional and vertical velocity components of the residual circulation, respectively. In general, the vertical component of the meridional circulation $\overline{w}^*$ is small compared to the meridional component $\overline{v}^*$ and so we neglect the vertical advection term for the purposes of this discussion. The first two terms on the right-hand side of (6) represent forcing of the zonal mean zonal winds by divergence of the EP fluxes associated with planetary-scale waves (F_p) and smaller-scale gravity waves (F_g) defined in section 4.5. The term $\overline{X}$ represents additional unresolved processes such as friction and eddy diffusion, which are not considered here.

[62] In the upper stratosphere and mesosphere, the TEM residual circulation during January is characterized by rising motion over the summer pole, cross-equatorial flow from summer to winter hemisphere, and sinking motion over the winter pole. In general, stronger planetary wave forcing in the extratropical winter stratosphere produces a stronger northward meridional circulation. However, if the planetary wave forcing is strong enough, it can lead to a breakdown of the westerly stratospheric polar vortex and produce a SSW. In the event of a major SSW such as the one on 20 January 2006, westerly flow in the extratropical stratosphere is replaced by easterly flow and upward propagation of planetary waves from the troposphere is inhibited.

[63] The influence of the planetary wave-driven residual meridional circulation on the tropical source region of the Q2DW can be seen by comparing the time behavior of $\overline{v}^*$ with that of the Q2DW eddy momentum fluxes at the 0.8 hPa level. Figure 16a plots values of $\overline{v}^*$ derived from the NOGAPS-ALPHA wind and temperature analyses that have been low-pass filtered to retain only zonal wave numbers 1–2. Also plotted in Figure 16a are the time variations in the Q2DW eddy momentum flux at 0.8 hPa from Figure 15a. Large positive (i.e., northward) values of $\overline{v}^*$ are seen between 15°N and 25°N on days 8–10, directly following the initial peak in the 100 hPa eddy heat flux (Figure 6). Although Figure 16a only extends to 25°N, it should be noted that the peak in $\overline{v}^*$ at 0.8 hPa extends up to 45°N (not shown).

[64] Using a band-pass filter to selectively isolate the contributions to $\overline{v}^*$ from zonal wave numbers 1–6, we have determined that the large peaks in $\overline{v}^*$ in Figure 16a are

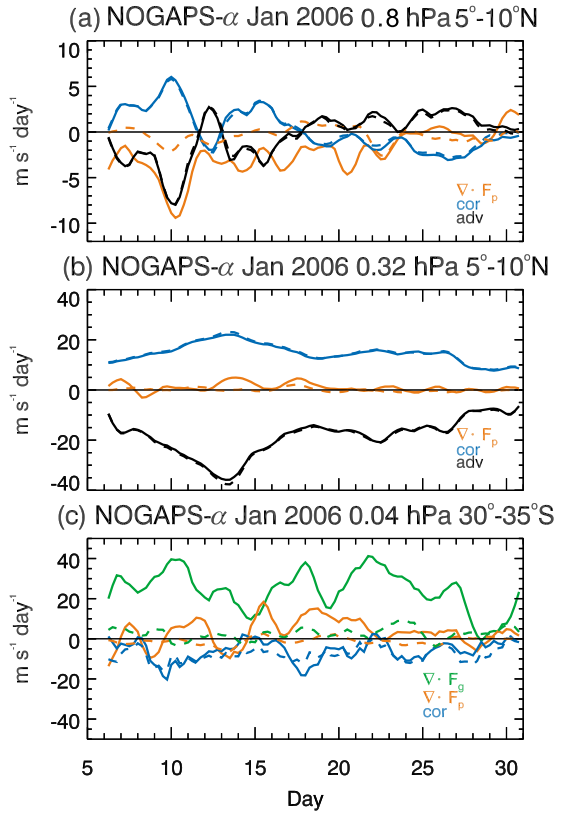

Figure 17. Contributions to the zonal wind tendency during 5–31 January 2006 from planetary waves (red), gravity waves (green), Coriolis torque (blue), and momentum advection (black) at (a) 0.8 hPa over 5°N–10°N, (b) 0.32 hPa over 5°N–10°N, and (c) 0.04 hPa over 30°S–355°S. Solid (dashed) curves are derived from the unfiltered (low-pass waves 1 and 2) NOGAPS-ALPHA analyses.

indeed related predominantly to zonal wave numbers 1 and 2. Figure 16a indicates that the increased planetary wave 1 and 2 forcing related to the large eddy heat flux in the extratropical lower stratosphere on 8–10 January (Figure 6) produces strong cross-equatorial flow near the equatorial stratopause. The peak in $\overline{v}^*$ near the equator on day 10 occurs within the inertially unstable region and coincides with the first peak in Q2DW eddy momentum flux at this level. We conclude that penetration of planetary waves 1–2 into the winter subtropical stratopause region strengthened the cross-equatorial component of the meridional residual circulation.

[65] Figure 16b plots the time variations in $\overline{v}^*$ computed from zonal wave numbers 1–2 within the equatorial null region at the 0.32 hPa level. We find a pronounced maximum in the northward component of $\overline{v}^*$ centered on 10°N on 12–13 January, ~2–3 days following the peak in $\overline{v}^*$ at the 0.8 hPa level in Figure 16a. Coincident with the peak in $\overline{v}^*$ at this level, both the (3, 1.9) critical line and the northern edge of the inertially unstable region push northward. Clearly, the strong planetary wave forcing of the mean meridional circulation in early January modified the inertially unstable region in the equatorial lower mesosphere.

[66] Figure 16c plots variations in $\overline{v}^*$ derived from the zonal wave 1–2 filtered NOGAPS-ALPHA analyses within the extratropical Q2DW source region at 0.04 hPa. Positive (northward) values are found in $\overline{v}^*$ between 20°S and 30°S from 5–10 January. Superimposed on the $\overline{v}^*$ contours in Figure 16c are the time variations in the Q2DW eddy heat flux at 0.04 hPa from Figure 15c. Unlike the results at the 0.8 hPa level in Figure 16a, we do not find evidence for a strong relationship between $\overline{v}^*$ anomalies and Q2DW forcing. As we will now show, this is due to the fact that the impact of changes in $\overline{v}^*$ on the background state in the extratropical upper mesosphere related to planetary wave activity in the NH are small in comparison with the effects of gravity wave breaking.

[67] To determine the dominant processes affecting the zonal wind tendency in each of the three regions described above, Figure 17 plots values of the individual terms in the zonal mean zonal wind tendency equation (6) computed from the NOGAPS-ALPHA horizontal wind and temperature fields for the month of January 2006. The calculations are first carried out using values of $\overline{v}^*$ and $\overline{w}^*$ obtained from the standard (unfiltered) NOGAPS-ALPHA meteorological fields in order to describe the contributions to the zonal wind tendency from all spatial scales (solid curves in Figure 17). The calculations are then repeated using values of $\overline{v}^*$ and $\overline{w}^*$ computed from low-pass filtered (zonal wave numbers 1 and 2) NOGAPS-ALPHA fields in order to isolate the contribution from the largest planetary wave modes (dashed curves in Figure 17).

[68] Figure 17a plots the largest terms in the zonal wind tendency equation within the tropical Q2DW source region computed from the unfiltered NOGAPS-ALPHA fields at 0.8 hPa between 5°N and 10°N. These are the planetary wave forcing ($\nabla \cdot \mathbf{F_p}$) (solid red curve) and horizontal momentum advection (solid black curve). Both terms show strong negative values (i.e., westward acceleration) peaking on 10 January. These terms are partially offset by the positive values (i.e., eastward acceleration) in the Coriolis term $f\,\overline{v}^*$, but the net effect is consistent with the increase in the strength of the easterly flow during mid-January seen in this region in Figure 15a. Contributions from vertical advection and gravity waves ($\nabla \cdot \mathbf{F_g}$) are quite small in comparison and not plotted in Figure 17a. A comparison of the planetary wave forcing derived from the full fields (solid red curve) with that derived from the low-pass filtered fields (dashed red curve) reveals that most of the planetary wave forcing comes from the higher zonal wave numbers. Additional calculations using a selective spatial filter to isolate individual wave numbers (not shown) confirm that the variations in $\nabla \cdot \mathbf{F_p}$ in Figure 17a are associated with the zonal wave number 3 Q2DW forcing in this region. In contrast, the contribution to the horizontal advection term is due almost entirely to the zonal wave number 1 and 2 components.

[69] Figure 17b examines the largest terms in the zonal wind tendency equation within the null region at the 0.32 hPa level averaged between 5°N and 10°N. Here the dominant term in the zonal wind tendency is the meridional advection term, which shows a peak easterly acceleration on 13 January. The close agreement between the results from the unfiltered analyses (solid curves) and from the low-pass filtered analyses (dashed curves) indicates that the contributions from zonal wave numbers 1 and 2 are driving the zonal wind tendencies at this level. The intensification and northward expansion of the summer easterly jet in Figure 15b

between 10 and 15 January can then be explained by increased northward advection of easterly momentum by $\overline{v}^*$ in response to the strong planetary wave activity in the northern subtropics, as seen in Figure 16b.

[70] Figure 17c plots the dominant terms in the momentum budget within the extratropical source region of the Q2DW at 0.04 hPa averaged between 30°S and 50°S. Unlike the lower levels, here $\nabla \cdot \mathbf{F_g}$ is by far the largest term in the zonal wind tendency. The contribution from horizontal advection is negligible and is not included in Figure 17c.

[71] Comparison of the time behavior of the $\nabla \cdot \mathbf{F_g}$ with the Q2DW eddy heat flux in the extratropical source region (Figure 15c) reveals some similarities but no strong relationship overall. For example, both the gravity wave tendency and the eddy heat flux peak on 10 January, decrease from 11 to 15 January, and then increase from 15 to 20 January. Furthermore, the peak $\nabla \cdot \mathbf{F_g}$ on 10 January in Figure 17c coincides with a peak in the Coriolis term determined from the low-pass filtered analyses. Since conditions determining gravity wave breaking are highly sensitive to variations in the background zonal wind, it's possible that small zonal wind perturbations caused by $\overline{v}^*$ anomalies related to zonal wave numbers 1 and 2 could impact gravity wave forcing of the zonal mean zonal winds, and thereby affect the baroclinically unstable source regions of the Q2DW. However, other peaks in the gravity wave term in Figure 17c on 18 and 22 January do not coincide with peaks in the Coriolis term, making it difficult to connect the daily variations in Q2DW forcing in the extratropical source region with changes in the residual meridional circulation related to wave numbers 1 and 2 throughout the entire month of January. Further investigation of the gravity wave forcing in the extratropical Q2DW source region will require detailed analysis of the zonal winds throughout the underlying atmospheric region, and is beyond the scope of this present paper.

6. Summary

[72] The NOGAPS-ALPHA high-altitude data assimilation system provides the first set of global synoptic meteorological analyses describing the evolution of the quasi 2-day wave in the middle atmosphere. Spectral analysis of NOGAPS-ALPHA assimilated winds, temperatures, and water vapor mixing ratios in the mesosphere shows pronounced zonal wave number 3 features propagating westward at frequencies near 0.5 cpd during the January 2006 period. Space-time filtering of these fields reveals peak monthly mean Q2DW amplitudes in mesospheric temperature, meridional wind, and water vapor of 8 K, 50 m s^{-1}, and 0.5 ppmv, respectively. The vertical and meridional structure of the Q2DW agrees well with earlier studies.

[73] EP-flux diagnostics based on space-time filtered NOGAPS-ALPHA wind and temperature fields show two distinct source regions for Q2DW activity. The first region lies along the equatorward flank of the summertime mesospheric easterly jet at midlatitudes. The large eddy heat fluxes associated with the Q2DW in this extratropical source region confirm that baroclinic instabilities provide the transient wave forcing that projects onto the global 2-day mode. The second source region is found near the tropical stratopause. Large eddy momentum fluxes in this region indicate that barotropic instability is the primary source of transient wave forcing for the Q2DW. These two source regions are separated by a "null" region in the subtropical mesosphere between ~0.3–0.6 hPa where EP fluxes associated with the Q2DW forcing are negligible.

[74] As in previous studies, the NOGAPS-ALPHA analyses show that the Q2DW is episodic in nature. During January 2006, the Q2DW amplitudes in meridional wind in both the extratropical and tropical source regions (Figure 10) display similar time behavior despite the differing natures of the forcing (i.e., baroclinic versus barotropic instability) within these two regions. Specifically, Q2DW amplitudes in v above the 0.1 hPa level peak throughout the summer mesosphere on 10 and 17 January, shortly after periods of strong planetary wave activity in the northern winter stratosphere. In the summer subtropical stratopause region, the amplitude of the Q2DW in vertical velocity increased immediately following the SSW on 20 January. Shortly thereafter, Q2DW amplitudes in H_2O in this region also increased.

[75] An analysis of the TEM residual circulation associated with zonal waves 1 and 2 shows a northward enhancement in $\overline{v}^*$ following an episode of strong planetary wave activity from 8 to 10 January. The resulting enhancement in meridional advection of easterly momentum across the equatorial stratopause is immediately followed by increased Q2DW forcing through the formation of barotropic instabilities in the tropical source region. Shortly thereafter, we find evidence of inertially unstable circulations in the equatorial lower mesosphere related to strong planetary wave activity in the subtropical upper stratosphere. The circulations created by the inertial instabilities drew the subtropical summer easterly jet equatorward and further intensified the curvature in the zonal wind field, thereby maintaining conditions favorable for Q2DW forcing via barotropic instability.

[76] In the extratropical Q2DW source region, there is some evidence that Coriolis torque related to an enhanced northward component in $\overline{v}^*$ on 10 January affected the zonal wind tendency, but this effect is small in comparison with the gravity wave forcing. These initial results indicate that planetary wave activity in the Northern winter stratosphere may have produced some zonal wind variations in the baroclinically unstable Q2DW source region in the extratropical upper mesosphere. However, detailed modeling studies are needed in order to clearly separate cause and effect before any definitive link can be made.

[77] Overall, the NOGAPS-ALPHA analyses for January 2006 indicate that enhanced planetary wave activity in the winter stratosphere prior to the SSW influenced the evolution of the Q2DW in horizontal winds, temperature, and water vapor mixing ratios. We are currently extending NOGAPS-ALPHA analyses to additional years in order to determine whether or not the relationship between stratospheric planetary wave activity and the behavior of the Q2DW in January 2006 is typical. It would be interesting, for example, to see if the Q2DW signal in H_2O near 1 hPa (Figure 7) is present in years without a stratospheric sudden warming.

[78] **Acknowledgments.** This work was supported by grants from the Office of Naval Research. High-altitude NOGAPS-ALPHA assimilation runs were made possible by a grant of computer time from the DOD High Performance Computing Modernization Program at the U.S. Air Force Research Laboratory and at the Naval Oceanographic Office. The authors

wish to thank the Aura MLS and TIMED SABER groups for providing access to their data.

References

Andrews, D. G., J. R. Holton, and C. B. Leovy (1987), *Middle Atmosphere Dynamics*, 489 pp., Academic Press, San Diego, Calif.

Chou, M.-D., and M. J. Suarez (2002), A solar radiation parameterization for atmospheric studies, *NASA Tech. Memo.*, *10460*, 52 pp.

Chou, M.-D., M. J. Suarez, X. Z. Liang, and M.-H. Yan (2001), A thermal infrared radiation parameterization for atmospheric studies, *NASA Tech. Memo.*, *104606*, 65 pp.

Coy, L. (1979), A possible 2-day oscillation near the tropical stratopause, *J. Atmos. Sci.*, *36*, 1615–1618.

Coy, L., S. Eckermann, and K. Hoppel (2008), Planetary wave breaking and tropospheric forcing as seen in the stratospheric sudden warming of 2006, *J. Atmos. Sci.*, *66*, 495–507, doi:10.1175/2008JAS2784.1.

Daley, R., and E. Barker (2001), NAVDAS: Formulation and diagnostics, *Mon. Weather Rev.*, *129*, 869–883.

Eckermann, S. D. (2009), Hybrid $\sigma-$p coordinate choices for a global model, *Mon. Weather Rev.*, *137*, 224–245.

Eckermann, S. D., K. W. Hoppel, L. Coy, J. P. McCormack, D. E. Siskind, K. Nielsen, A. Kochenash, M. H. Stevens, and C. R. Englert (2009), High-altitude data assimilation system experiments for the Northern Hemisphere summer mesosphere season of 2007, *J. Atmos. Sol. Terr. Phys.*, *71*, 531–551.

Fomichev, V. I., J.-P. Blanchet, and D. S. Turner (1998), Matrix parameterization of the 15 μm CO_2 band cooling in the middle and upper atmosphere for variable CO_2 concentrations, *J. Geophys. Res.*, *103*(D10), 11,505–11,528.

Garcia, R. R., R. Lieberman, J. M. Russell, and M. G. Mylnczak (2005), Large-scale waves in the mesosphere and lower thermosphere observed by SABER, *J. Atmos. Sci.*, *62*, 4384–4399.

Garcia, R. R., D. R. Marsh, D. E. Kinnison, B. A. Boville, and F. Sassi (2007), Simulation of secular trends in the middle atmosphere, *J. Geophys. Res.*, *112*, D09301, doi:10.1029/2006JD007485.

Harris, T. J. (1994), A long-term study of the quasi-two-day wave in the middle atmosphere, *J. Atmos. Terr. Phys.*, *56*, 569–579.

Hayashi, Y. (1971), A generalized method of resolving disturbances into progressive and retrogressive waves by space Fourier and time cross-spectral analyses, *J. Meteorol. Soc. Jpn.*, *49*, 125–128.

Hitchman, M. H., C. B. Leovy, J. C. Gille, and P. L. Bailey (1987), Quasi-stationary zonally asymmetric circulations in the equatorial lower mesosphere, *J. Atmos. Sci.*, *44*, 2219–2236.

Hogan, T., and T. Rosmond (1991), The description of the Navy Operational Global Atmospheric Prediction System's spectral forecast model, *Mon. Weather Rev.*, *119*, 1786–1815.

Hoppel, K. W., N. L. Baker, L. Coy, S. D. Eckermann, J. P. McCormack, G. Nedoluha, and D. E. Siskind (2008), Assimilation of stratospheric and mesospheric temperatures from MLS and SABER in a global NWP model, *Atmos. Chem. Phys. Discuss.*, *8*, 8455–8490.

Lambert, A., et al. (2007), Validation of the Aura Microwave Limb Sounder middle atmospheric water vapor and nitrous oxide measurements, *J. Geophys. Res.*, *112*, D24S36, doi:10.1029/2007JD008724.

Lieberman, R. S. (1999), Eliassen-Palm fluxes of the 2-day wave, *J. Atmos. Sci.*, *56*, 2846–2861, (see also Lieberman, R. S. (2002), Corrigendum, *J. Atmos. Sci.*, *59*, 2625–2627.

Limpasuvan, V., and C. Leovy (1995), Observation of the two-day wave near the southern summer stratopause, *Geophys. Res. Lett.*, *22*(17), 2385–2388.

Limpasuvan, V., and D. L. Wu (2003), Two-day wave observations of UARS Microwave Limb Sounder mesospheric water vapor and temperature, *J. Geophys. Res.*, *108*(D10), 4307, doi:10.1029/2002JD002903.

Limpasuvan, V., and D. L. Wu (2009), Anomalous two-day wave behavior during the austral summer, *Geophys. Res. Lett.*, *36*, L04807, doi:10.1029/2008GL036387.

Limpasuvan, V., C. B. Leovy, Y. J. Orsolini, and B. Boville (2000a), A numerical simulation of the two-day wave near the stratopause, *J. Atmos. Sci.*, *57*, 1702–1717.

Limpasuvan, V., C. B. Leovy, and Y. J. Orsolini (2000b), Observed temperature two-day wave and its relatives near the stratopause, *J. Atmos. Sci.*, *57*, 1689–1701.

Limpasuvan, V., D. L. Wu, M. J. Schwartz, J. W. Waters, Q. Wu, and T. L. Kileen (2005), The two-day wave in EOS MLS temperature and wind measurements during 2004–2005 winter, *Geophys. Res. Lett.*, *32*, L17809, doi:10.1029/2005GL023396.

Madden, R. A., and P. R. Julian (1971), Detection of a 40–50 day oscillation in the zonal wind in the tropical Pacific, *J. Atmos. Sci.*, *28*, 702–708.

McCormack, J. P., S. D. Eckermann, D. E. Siskind, and T. J. McGee (2006), CHEM2D-OPP: A new linearized gas-phase ozone photochemistry parameterization for high-altitude NWP and climate models, *Atmos. Chem. Phys.*, *6*, 4943–4972.

McCormack, J. P., K. H. Hoppel, and D. S. Siskind (2008), Parameterization of middle atmospheric water vapor photochemistry for high-altitude NWP and data assimilation, *Atmos. Chem. Phys. Discuss.*, *8*, 13,999–14,032.

Muller, H. G., and L. Nelson (1978), A traveling quasi 2-day wave in the meteor region, *J. Atmos. Terr. Phys.*, *40*, 761–766.

Norton, W. A., and J. Thuburn (1999), Sensitivity of mesospheric mean flow, planetary waves, and tides to strength of gravity wave drag, *J. Geophys. Res.*, *104*(D24), 30,897–30,911.

Orsolini, Y. J., V. Limpasuvan, and C. B. Leovy (1997), The tropical stratopause response in the UKMO stratospheric analyses: Evidence for a 2-day wave and inertial circulations, *Q. J. R. Meteorol. Soc.*, *123*, 1707–1724.

Palmer, T. N., G. J. Shutts, and R. Swinbank (1986), Alleviation of a systematic westerly bias in general circulation and numerical weather prediction models through an orographic gravity wave drag parameterization, *Q. J. R. Meteorol. Soc.*, *112*, 1001–1039.

Plumb, R. A. (1983), Baroclinic instability of the summer mesosphere: A mechanism for the quasi-two-day wave?, *J. Atmos. Sci.*, *40*, 262–270.

Randel, W. J. (1993), Global normal-mode Rossby waves observed in stratospheric ozone data, *J. Atmos. Sci.*, *50*, 406–420.

Randel, W., et al. (2004), The SPARC inter-comparison of middle-atmosphere climatologies, *J. Clim.*, *17*, 986–1003.

Remsberg, E. E., et al. (2008), Assessment of the quality of the Version 1.07 temperature-versus-pressure profiles of the middle atmosphere from TIMED/SABER, *J. Geophys. Res.*, *113*, D17101, doi:10.1029/2008JD010013.

Richter, J. H., F. Sassi, R. R. Garcia, K. Matthes, and C. A. Fischer (2008), Dynamics of the middle atmosphere as simulated by the Whole Atmosphere Community Climate Model, version3 (WACCM3), *J. Geophys. Res.*, *113*, D08101, doi:10.1029/2007JD009269.

Rodgers, C. D., and A. J. Prata (1981), Evidence for a traveling two-day wave in the middle atmosphere, *J. Geophys. Res.*, *86*(C10), 9661–9664.

Salby, M. L. (1981), The 2-day wave in the middle atmosphere: Observations and theory, *J. Geophys. Res.*, *86*(C10), 9654–9660.

Salby, M. L., and P. F. Callaghan (2001), Seasonal amplification of the 2-day wave: Relationship between normal mode and instability, *J. Atmos. Sci.*, *58*, 1858–1869.

Salby, M. L., and P. F. Callaghan (2003), Dynamics of the 2-day wave in a nonlinear model of the middle atmosphere, *J. Geophys. Res.*, *108*(D23), 4713, doi:10.1029/2003JD003648.

Sassi, F., R. R. Garcia, and B. A. Boville (1993), The stratopause semi-annual oscillation in the NCAR community climate model, *J. Atmos. Sci.*, *50*, 3608–3624.

Schwartz, M. J., et al. (2008), Validation of the Aura Microwave Limb Sounder temperature and geopotential height measurements, *J. Geophys. Res.*, *113*, D15S11, doi:10.1029/2007JD008783.

Thompson, R. (1979), Coherence significance levels, *J. Atmos. Sci.*, *36*, 2020–2021.

von Storch, H., and F. W. Zwiers (1999), *Statistical Analysis in Climate Research*, 484 pp., Cambridge Univ. Press, New York.

Wu, D. L., P. B. Hays, R. W. Skinner, A. R. Marshall, M. D. Burrage, R. S. Lieberman, and D. A. Ortland (1993), Observations of the quasi 2-day wave from the High Resolution Doppler Imager on UARS, *Geophys. Res. Lett.*, *20*(24), 2853–2856.

L. Coy and J. P. McCormack, Space Science Division, Naval Research Laboratory, 4555 Overlook Avenue, SW, Washington, DC 20375, USA. (john.mccormack@nrl.navy.mil)

K. W. Hoppel, Remote Sensing Division, Naval Research Laboratory, 4555 Overlook Avenue, SW, Washington, DC 20375, USA.